# ELECTRONIC PROGRESS

RAYTHEON

*in this issue:*

D. H. HILL LIBRARY
FEB 28 1961
North Carolina State College

VOLUME V NOVEMBER - DECEMBER 1960 NUMBER 3

# ELECTRONIC PROGRESS

Copyright 1961, Raytheon Company, Waltham 54, Mass.

RAYTHEON


**1** Microwave Heat Exchanger · *Robert Gartland*

**14** Inventions

**15** Papers and Publications

**15** Technical Publications Panel .

**16** A High Power Microwave Rectifier *John Skowron, James Thomas*

**22** Statistical Analysis as an Engineering Tool, Part Two . . . . *Maurice Prendergast*



*Martin Schilling* ..... EXECUTIVE EDITOR
*Michael A. Walker* ..... MANAGING EDITOR
*Frances Dal Corobbo* ..... EDITOR
*William Niles* ..... ART EDITOR

*Printed in U.S.A.*



**EDITORIAL ADVISORY BOARD**

*Laurence Batchelder*
*Submarine Signal Operations*

*Thomas P. Cutler*
*Missile Systems Division*

*Robert Edwards*
*Microwave and Power Tube Division*

*John D. Harmer*
*Airborne Electronic Equipment Operations*

*Melvin G. Holland*
*Research Division*

*John E. Meade*
*Surface Radar and Navigation Operations*

*Gordon R. Partridge*
*Communications and Data Processing Operations*

*William L. Root, Jr.*
*Commercial Apparatus and Systems Division*

*John H. Shea*
*Semiconductor Division*


**COVER**

*The direct conversion of high power microwave energy into usable heat is one facet of Raytheon's efforts in super power microwave technology. Our cover presents an artist's conception of a microwave heat exchanger, which is described in detail in the feature article in this issue.*

Figure 1. Conceptual Design of a Microwave Heat Exchanger

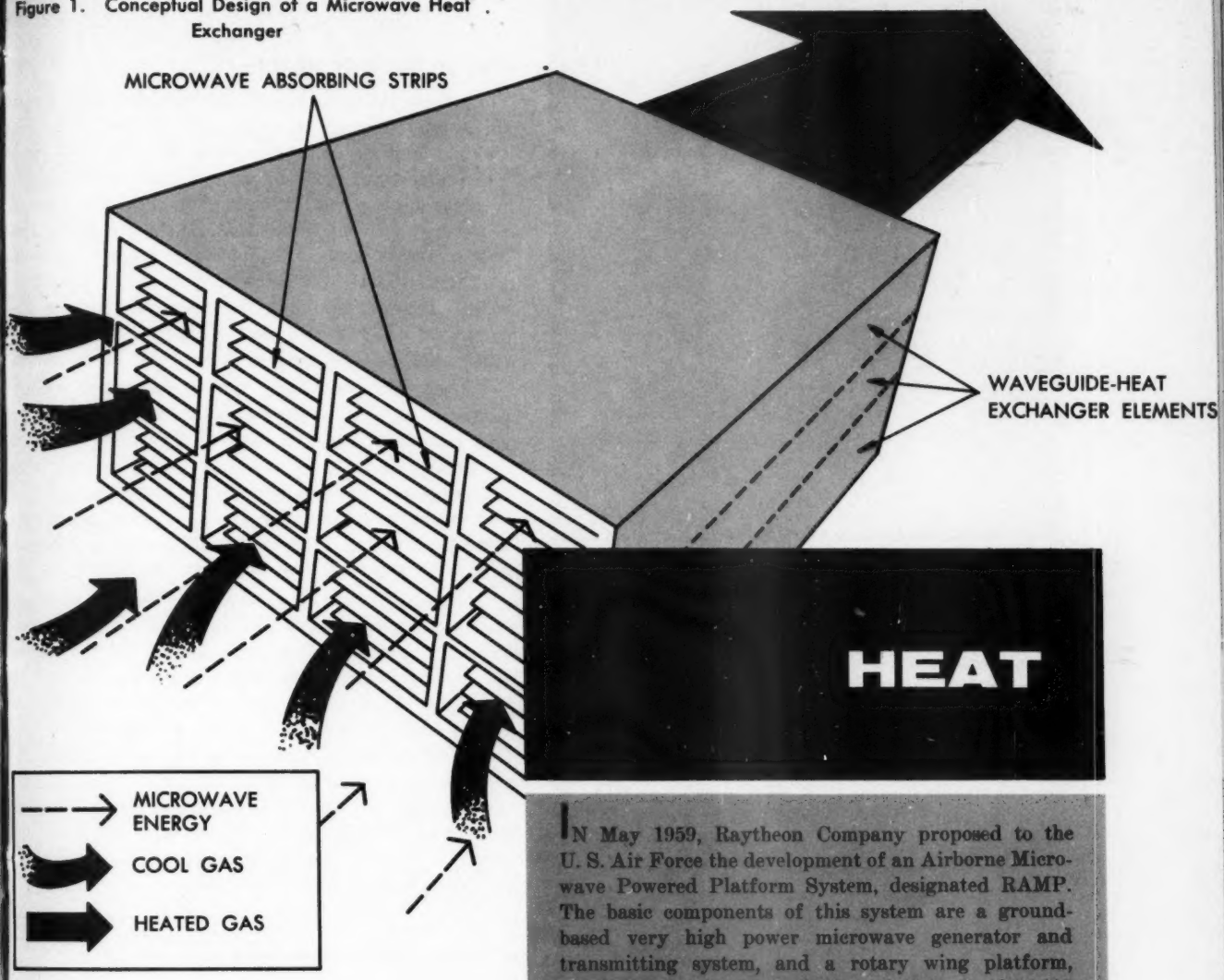


IN May 1959, Raytheon Company proposed to the U. S. Air Force the development of an Airborne Microwave Powered Platform System, designated RAMP. The basic components of this system are a ground-based very high power microwave generator and transmitting system, and a rotary wing platform, which is capable of hovering at an altitude of 65,000 feet for periods of weeks. Microwave energy is generated on the ground and beamed to a receiving antenna on the platform where it is collected and transmitted to a microwave heat exchanger. The electrical energy is converted into thermal energy in the heat exchanger and transferred to the working fluid of a gas turbine engine, which develops primary power for the vehicle.

This proposed use of microwave energy is a forerunner of many conceivable applications of the wireless transmission of power. For example, microwave energy can be transmitted between ground stations and converted into heat to power a gas turbine, whose output could be used to generate power frequencies or to do other forms of work. Microwave energy can be converted directly to electrical energy at power frequencies by utilizing the thermoelectric effect. In this case, thermoelectrically efficient thermocouples would be made integral with the microwave heat exchanger.

**ROBERT H. GARTLAND** *is a Senior Engineer in the Servo Mechanics Department, Airborne Systems Operations. His industrial experience prior to joining Raytheon has included studies of theoretical thermodynamics and atomic weapons effects on aircraft and missiles as well as research and development work on advanced fighter aircraft and weather radars. Since he joined Raytheon in 1957, he has worked on cooling system designs of the B-58 Hustler doppler radar and on development of the microwave heat exchanger. Mr. Gartland received his B.S. degree in Mechanical Engineering from the University of Rhode Island in 1952 and has completed his academic work on the M.S. degree in Physics at Northeastern University.*

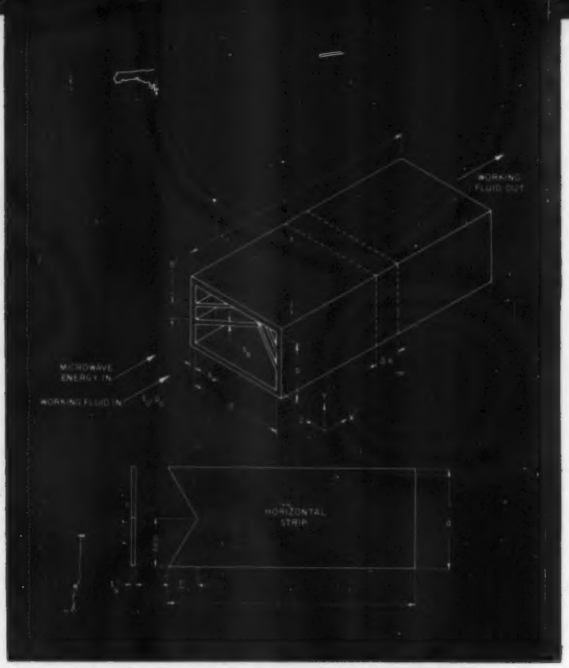


**Figure 2. Typical Heat Exchanger Unit**

Here the converted microwave energy would be used to provide heat for the hot thermocouple junctions. Direct conversion of microwave energy could also be accomplished by using thermionic effects. For this application, the heated wall of the heat exchanger would serve as a cathode in much the same fashion as a vacuum tube cathode. It is also conceivable that direct conversion of microwave energy could be brought about by using the microwave heat exchanger with a magnetohydrodynamic generator. In this system the microwave energy would be used to provide heat for ionization of the working gas, which would then be passed through a magnetic field; electrodes then pick off the direct current generated.

Many problems remain to be solved before microwave energy can be beamed and collected efficiently at very high energy levels, not only between ground stations but from ground to space. This article presents the engineering considerations involved in designing a microwave heat exchanger, including an analytical definition of microwave power attenuation in the geometry of a heat exchanger, an investigation of materials suitable for this application, and a heat transfer analysis. The results of the analytical study have been used to develop preliminary design criteria, and the more important analytical conclusions have been substantially verified by experimental measurements carried out on especially constructed breadboard units. Some problems require further work before a sufficient background of engineering data is accumulated to permit the design and construction of a microwave heat exchanger capable of supplying heat for realistic applications. There is no doubt, however, that the feasibility of such a device has been established.

## Design Considerations

Problems encountered in the analysis and design of a microwave heat exchanger involve electrical, thermal, and mechanical criteria. The device is much more than a dummy load since it must absorb all the incident high power microwave energy and convert the energy efficiently into heat. It must transfer this heat to a working fluid without exceeding the temperature limitations of the material from which it is fabricated. It must minimize the pressure drop on the system of which it is a part. Lastly, it must be of a reasonable size and weight, at least for airborne use.

In the heat exchanger under study, the energy contained in the microwave radiation is absorbed by heat transfer surfaces inside a waveguide, from which it is transferred to the working fluid of the gas turbine engine. The working fluid passes through the waveguide in the same direction as that of the microwave propagation. The conceptual design is shown in Figure 1; a typical unit is shown in Figure 2.

One consideration in the design is the rate at which the microwave energy is absorbed by the surfaces. This is dependent upon the geometry of the device and the frequency of the microwave energy as well as upon the microwave properties of the material. A second consideration is the transfer of thermal energy from the absorbing surfaces to the working fluid at the flow rate required. This similarly depends upon the geometry of the surfaces but also upon the temperature difference between the surfaces and the working fluid. General design considerations are treated in detail in the following sections.

### Microwave Energy Absorption in Rectangular Waveguide

Microwave energy being propagated down a waveguide is always attenuated to some degree in the walls of the waveguide. This attenuation can be augmented in two ways. Horizontal strips of the waveguide material can be placed in the waveguide perpendicular to the electric field (parallel to the waveguide's long side). Such attenuation is called conductor loss. A second type of attenuation, dielectric loss, can be obtained by placing dielectric material in the waveguide parallel to the electric field (perpendicular to the long side). After analyzing these two attenuation techniques, it was decided to base the heat exchanger design on the conductor loss method. Three factors dictated this choice: the theoretical analysis was less involved, electrical matching presented fewer problems, and heat exchanger fabrication was simplified.

The differential equation describing the power dissipation in a waveguide with no horizontal strips is given by:

$$\frac{dP}{dx} = -2\alpha_g P, \qquad (1)$$

where $\alpha_g$ (the attenuation constant for the waveguide) is given by:

$$\alpha_g = \frac{R_s}{b\sqrt{\frac{\mu_o}{\epsilon_o}}} \frac{\lambda_g}{\lambda}\left[1 + \frac{2b}{a}\left(\frac{\lambda}{\lambda_c}\right)^2\right]. \qquad (2)$$

Now, since $R_s = \frac{1}{\sigma\delta} = \frac{\rho}{\delta}$,

$$\delta = \sqrt{\frac{1}{\pi f \mu \sigma}} = \sqrt{\frac{\rho}{\pi f \mu}}, \qquad (3)$$

and $\lambda_c = 2a$ for the $TE_{10}$ mode, simple substitution of these relationships into Equation 2 gives the following result for $\alpha_g$:

$$\alpha_g = 7.5\sqrt{\rho}\sqrt{f}\frac{\lambda_g}{\lambda}\left[0.002222\left(\frac{1}{b}\right) + \left(\frac{1}{a^3}\right)\left(\frac{1}{f^2}\right)\right]. \qquad (4)$$

If n horizontal strips are inserted into the waveguide, and each are at least twice as thick as the skin depth (i.e., $t \geq 2\delta$) the attenuation constant $\alpha_g'$, becomes in this case:

$$\alpha_g' = 7.5\sqrt{\rho}\sqrt{f}\frac{\lambda_g}{\lambda}\left[0.002222\left(\frac{1}{b'}\right) + \left(\frac{1}{a^3}\right)\left(\frac{1}{f^2}\right)\right]. \qquad (5)$$

The equation describing the attenuation becomes:

$$\frac{dP}{dx} = -2\alpha_g' P. \qquad (6)$$

In other words, the attenuation constant is increased by decreasing the vertical height, or:

$$\alpha_g' \approx \left(\frac{b}{b'}\right)\alpha_g. \qquad (7)$$

It is shown that, for operation at a given frequency and a fixed waveguide cross section, the power dissipation per unit length can be changed by varying the resistivity and number of the horizontal strips. The power distribution along the waveguide for a typical case is shown in Figure 3. The calculations were made for a frequency of 10.1 kmc. These results show that a material resistivity of 0.1 to 1.0 ohm-centimeter should be used to dissipate the microwave energy within a reasonable distance along the waveguide (reasonable being defined as up to 48 inches).

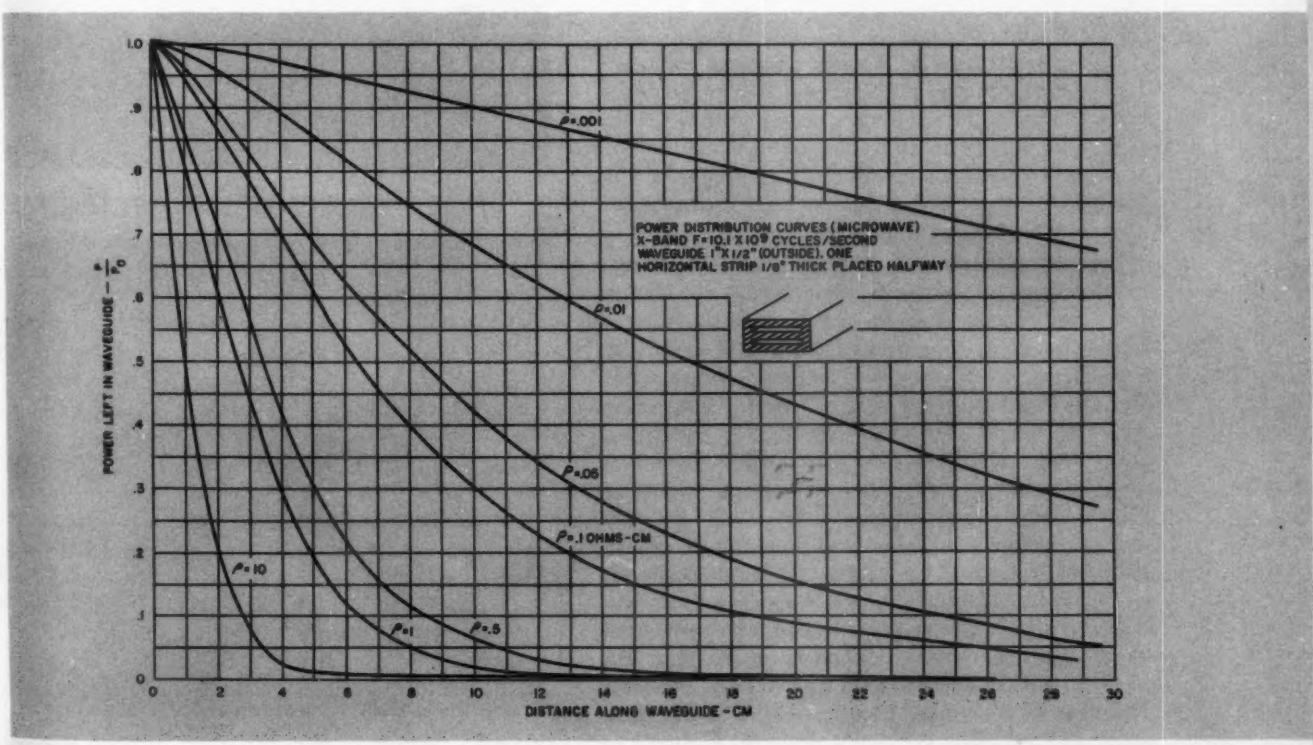


Figure 3. Power Distribution Curves, X-Band, One Horizontal Strip

The thickness of the strips selected for these calculations was determined by its effect on the heat transfer to the working fluid, although the use of thicker strips would have resulted in more rapid absorption of the power along the waveguide.

A consideration arising from the use of the dissipating strips, however, is that if the strips were suddenly introduced at a point in the waveguide, the resulting mismatch would reflect much of the microwave power. This mismatch can be reduced by stepping sections in the horizontal strips a quarter wavelength apart or by gradual transmission from the free waveguide to the dissipating medium by tapering. To minimize mismatch, linear V-shaped tapers were used for this analysis. The length of the taper was made equal to or greater than the critical wavelength of the waveguide. Thus, over the tapered transistion region, the attenuation constant, $\alpha_{gt}$, was assumed to vary linearly between the value with no strips and the value with full strips; i.e.,

$$\alpha_{gt} = \alpha_g + \frac{\alpha_g' - \alpha_g}{\Sigma} (\Delta\Sigma). \qquad (8)$$

These theoretical considerations indicated that the taper would permit standing wave ratios of less than 1.1.

#### Materials

The material used in a microwave heat exchanger has definite requirements: its resistivity must be sufficient to absorb the microwave energy within the distance allowed, and it must be capable of withstanding the high temperatures involved in the energy transfer. Its structural properties and the ability to fabricate and assemble it are also important.

Ceramic materials seemed best to fulfill the material requirements of the heat exchanger at the desired frequency. Figure 4 shows how the resistivity varies for a selected number of ceramic materials — recrystallized silicon carbide, stabilized zirconia, chromic oxide, and an alumina-chromic oxide-magnesia composition. Although zirconia has a high resistivity, it occurs in a monoclinic form which cannot be used in fabricated shapes because it undergoes a structure-weakening volume change when heated to 1000°C. By the addition of calcium oxide, however, this volume change can be stabilized and the material made relatively easy to fabricate. Stabilized chromic oxide or alumina-chromic oxide-magnesia compositions are also subject to material temperature limitations in the neighborhood of 1000°C. The principal disadvantage of silicon carbide is its exceptional hardness, which makes fabrication difficult. The two types shown in Figure 4 — a green or n-type and a black or p-type — can be

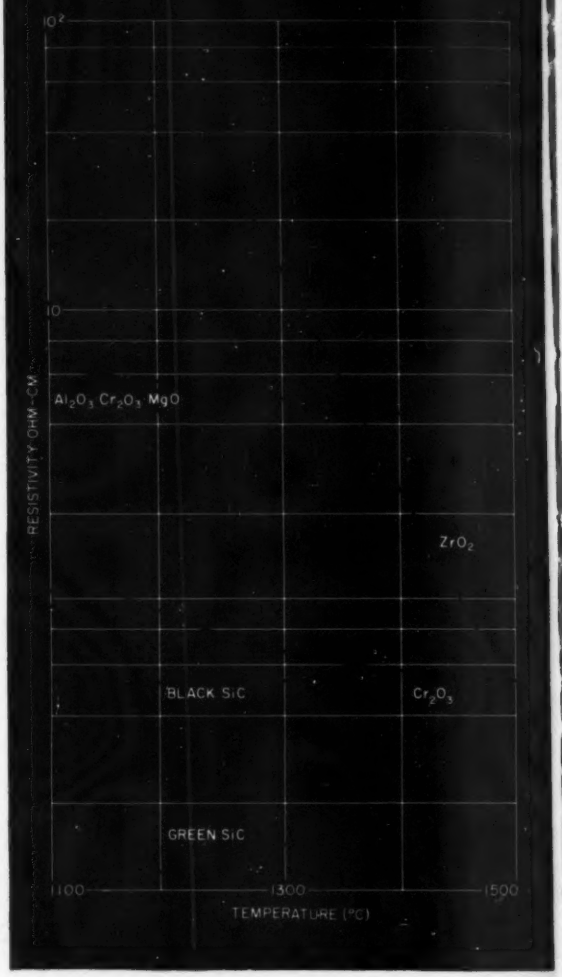


Figure 4. Resistivity Properties of Various Ceramics

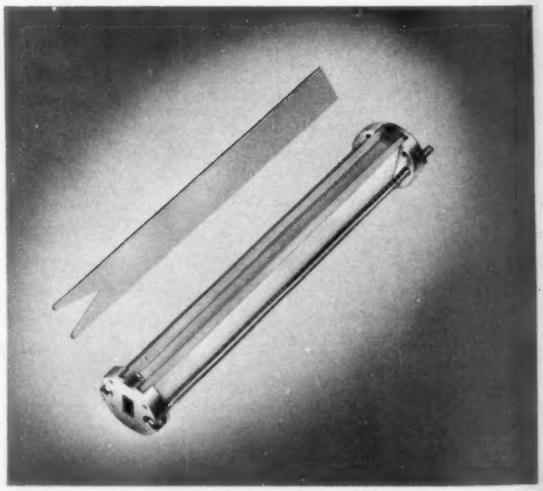

Figure 5. Crystallon-R Heat Exchanger Showing Tapered Horizontal Strip

combined to form materials with intermediate resistivities. The materials used in the experiments (Niafrax and Crystallon R) were all of the silicon carbide family. Although they are difficult to machine, these materials can be cast into a variety of shapes with good tolerance, are all capable of operating at temperatures up to 4200°F, and have thermal conductivities ranging from 100 to 300 Btu-in./(hr-ft²-°F).

The possibility of using more easily fabricated metals, such as stainless steel or a super alloy, was also investigated. It was found that a waveguide made of Inconel X would dissipate some power but would be unsatisfactory as an exchanger because its resistivity is too low to attenuate the incident microwave power in a reasonable length of waveguide. Even with as many as eight lossy strips in the waveguide, there would still be 48 per cent of the original energy left unattenuated in a length of 43 to 44 inches.

#### Thermodynamic Considerations

The problem of absorbing microwave energy is not new because attenuators, dummy loads, and matched terminations are common devices. What is new in a microwave heat exchanger is the problem of absorbing high levels of microwave energy in a relatively small device and transferring this energy efficiently to a working fluid, as well as minimizing the size and weight for airborne use.

The first thermodynamic design consideration involved selecting a particular heat exchanger system. Of the three general types — direct transfer, liquid coupled indirect transfer, and periodic flow — the direct transfer type was selected as the one which would result in minimum size and weight.

In a conventional direct transfer type of heat exchanger, two fluids (one hot, one cold) which exchange thermal energy, are physically separated by a heat

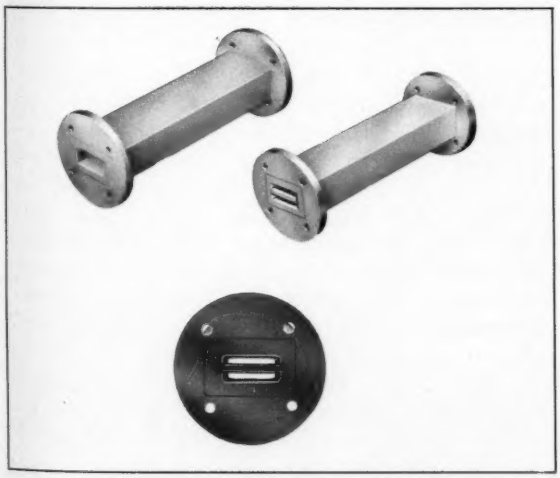

Figure 6. Niafrax Heat Exchanger

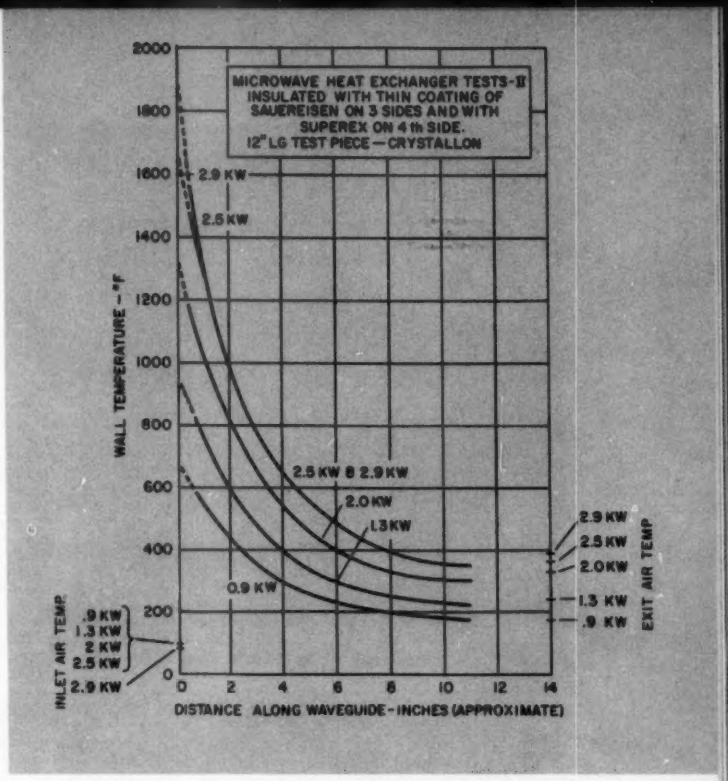


Figure 7. Crystallon-R Heat Exchanger Test Results

transfer surface. In a microwave energized system, however, the microwave energy, which acts like the hot fluid and gives up its energy to the heat transfer surface, is not physically separated from the working fluid. It is possible to physically separate the microwave energy from the working fluid, but in this case nothing would be gained, since the presence of the working fluid at high pressure promotes the propagation of high microwave energy levels.

Of the two types of working fluid flow operation possible, parallel to or opposite to the direction of the microwave energy propagation, the parallel type of operation was arbitrarily chosen for analysis.

In conventional heat exchanger design practice, a design is generated by determining the heat transfer surface area necessary to transfer a given amount of energy to a specified working fluid mass flow rate. The heat transfer surface area required for a microwave heat exchanger for a given energy level and working fluid flow rate is dependent on the microwave propagation frequency and heat exchanger material resistivity. The frequency determines the cross-sectional dimensions a and b (see Figure 2), and the material resistivity determines the number and spacing of the fins along with L, the length of the heat exchanger. Thus, once propagation frequency and material resistivity are specified the heat transfer surface area is fixed. Then, for a given working-fluid mass flow rate and energy transfer, the governing factors become the operating temperature of the heat transfer

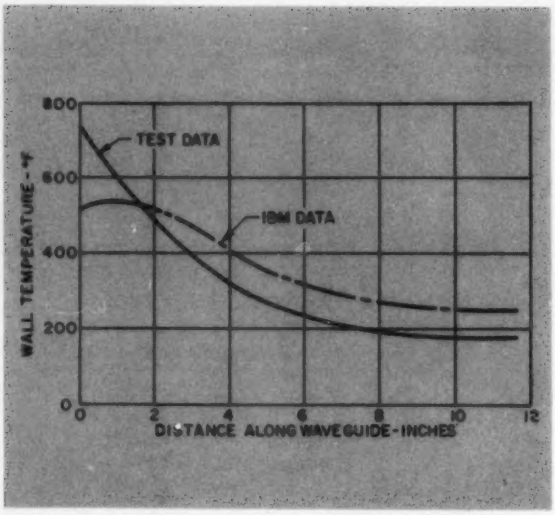


Figure 8. Comparison of Test Data and Theoretical Data

surface area and the pressure drop of the working fluid.

The basic heat transfer problem is the following: given a system consisting of a waveguide-like envelope containing horizontal fins and with a fixed amount of RF energy entering the envelope and given working fluid flow rate, it is required to define qualitatively the geometry and resulting temperature rise that will efficiently transfer the RF energy to a working fluid passing through the envelope. The term efficiently is not used here in the sense of efficiency or heat exchanger effectiveness. Transferring heat efficiently depends on the use of the heat exchanger. What is practicable and efficient for ground use may be unworkable for airborne use, because of size and weight. The pressure drop of the working fluid in passing through the heat exchanger can be too large despite a very high heat exchanger effectiveness. The heat exchanger wall temperature can be too high in an otherwise well designed heat exchanger. Thus, it should be clear that several variables enter into a heat exchanger design depending upon its intended application.

The accompanying heat transfer analysis presents the pertinent equations along with their derivations for a parallel flow heat exchanger of arbitrary geometry. These equations are for the steady state case and require only slight modifications for counter flow operation.

## Experimental Test Program and Results

The experimental program was directed toward the transfer of 3-kw CW power to a working fluid (air for this case) in a typical heat exchanger. A microwave frequency of 10.1 kmc was used for testing because of

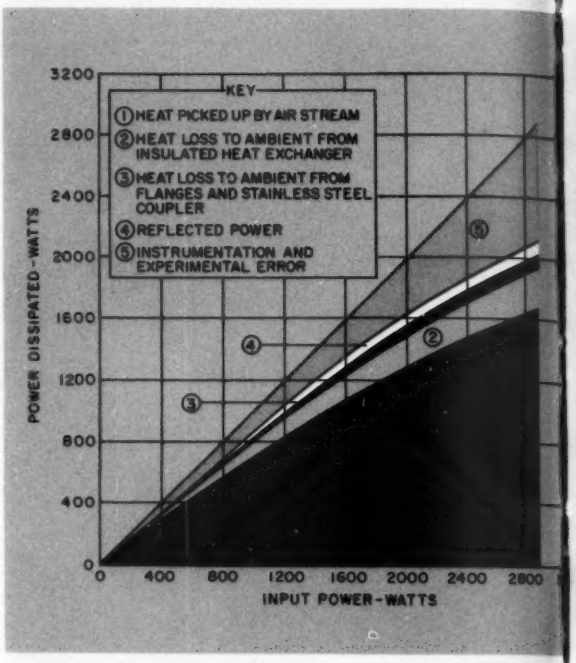


Figure 9. Heat Balance for Heat Exchanger Tests

the favorable operation of the Raytheon Amplitron at this frequency. Based on the results of the analytical and material studies, the experimental heat exchangers were simple silicon carbide waveguides having lossy walls and lossy strips across the wide dimensions of the waveguide. Both experimental models were of X-band frequency, 1/2 by 1 inch in cross section, with the center-fin thickness roughly 1/8 inch. The lengths of the models were determined from the microwave attenuation data shown in Figure 3, and were chosen so that more than 95 per cent of the entering microwave energy was attenuated in the heat exchanger.

### Heat Exchanger Models

The first heat exchanger fabricated is shown in Figure 5. It was constructed by fastening three horizontal planes of Crystallon-R silicon carbide between milled side plates. Stainless steel flanges were used for the terminations. Coupling of the heat exchanger to the stainless steel feeder waveguide was achieved through a low-loss cover flange. The use of a simple butt junction for this coupling would have required very careful mating to prevent current flow in the area between the two flanges. A choke flange, normally used to reduce the mechanical tolerances, was not used here because of the high loss which would occur in a resonant slot of lossy material. The length of the heat exchanger unit was 12 inches, and the resistivity for the material was 1 ohm-cm at 2,000°F. The calculated high-temperature attenuation for this design was better than 40 db.

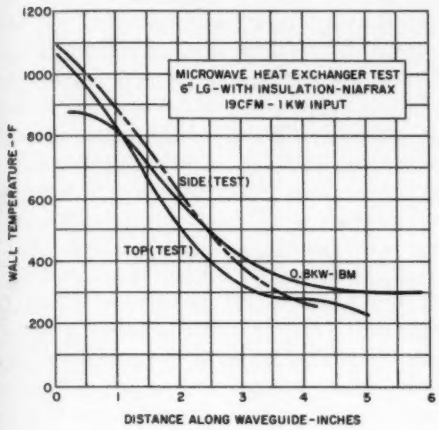
MICROWAVE HEAT EXCHANGER TEST
6" LG - WITH INSULATION - NIAFRAX
19CFM - 1 KW INPUT
SIDE (TEST)
TOP (TEST)
0.8KW - BM
WALL TEMPERATURE - °F
DISTANCE ALONG WAVEGUIDE - INCHES

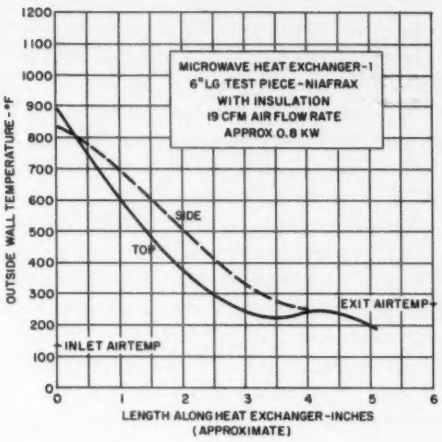


**Figure 10. Niafrax Heat Exchanger Test Results**

The second heat exchanger, including the input cover flange, was entirely fabricated of Niafrax (see Figure 6). The heat exchanger and the cover flange were fired as one piece. The junction to the stainless steel waveguide section consisted of a flat metal flange rigidly bolted to a flat silicon carbide flange. The length of this second exchanger was 6 inches, with a resistivity of approximately 2 ohm-cm at 2,500°F. The calculated minimum high-temperature attenuation was 45 db.

The microwave characteristics of the two heat exchanger models are listed in Table 1.

Table 1. Microwave Characteristics of Heat Exchanger Models

| | Crystallon-R, 12-inch | Niafrax, 6-inch |
|---|---|---|
| VSWR for 154-mw power input | 1.16 | 1.08 |
| VSWR for 3-kw power input | $< 1.5$ | $< 1.5$ |
| Insertion loss | 50 db | 47 db |

### Test Instrumentation

The instrumentation for the heat transfer tests was arranged as follows. The microwave energy was transmitted and monitored from the Amplitron through a stainless steel waveguide section into the heat exchanger where it was absorbed and converted to heat. (Stainless steel was used because of its low microwave power attenuation and its relatively high melting point.) The thermocouples were located on the two adjacent outside surfaces of one heat exchanger, spaced approximately 1 inch apart.

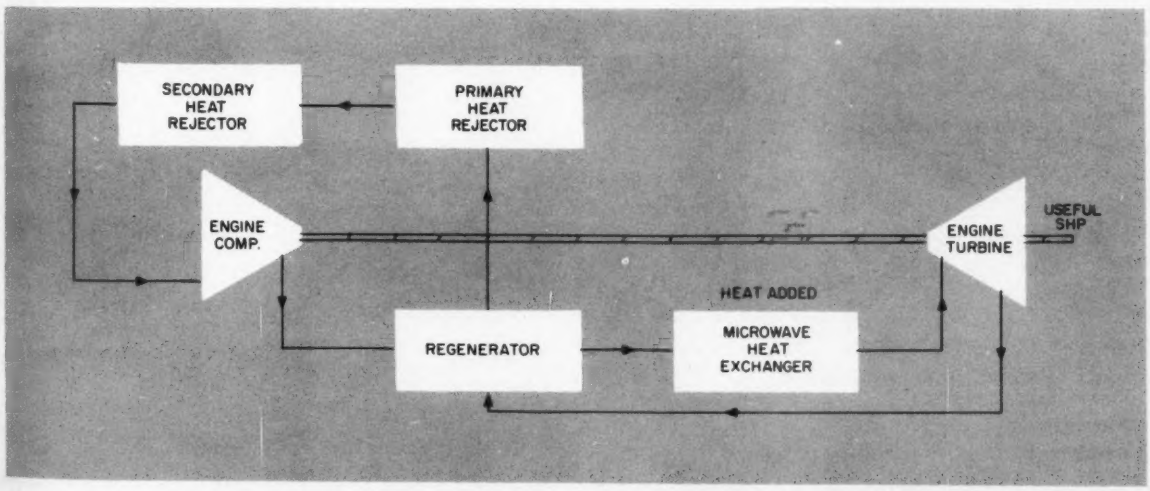


**Figure 11. Flow Diagram for a Typical Closed-Cycle Gas Turbine**

The thermocouples were made of chromel-alumel and were bound to the heat exchanger surfaces with Carborundum's Sauereisen 78, a ceramic cement. In installing the thermocouples, the heat exchanger surface was roughened slightly, the thermocouples were pressed against the surface, and Sauereisen 78 was applied over the thermocouples which were held in place until the Sauereisen 78 solidified. Because Sauereisen is a good insulator, care was taken to insure that none of it got between the thermocouple and the heat exchanger wall which would have resulted in wall temperatures lower than the true values. A Bristol multi-point recorder was used to monitor the wall temperatures.

The exit air thermocouple was positioned in the center of a duct, which was clamped to the existing flange of the heat exchanger. The inlet air thermocouple was mounted in the center of the air line before the microwave-to-air coupling section. The inlet and exit air thermocouples were made of chromel-alumel. Both air temperatures were monitored on a Leeds and Northrup potentiometer. Forced air was supplied by a blower with a capacity of 5 lbs/min, and the air flow rate was monitored by a Brooks rotameter. A static pressure probe was inserted into the stainless steel coupler and connected to a mercury manometer, permitting an accurate determination of the pressure drop across the heat exchanger.

#### Microwave Components

A QK410-622 prototype CW magnetron with its associated constant-current supply was used to generate 150 to 200 watts at 10.1 kmc. This signal was amplified by a QK680 Amplitron which was isolated from the magnetron to protect the latter from reflected or spurious signals. The Amplitron was operated at maximum gain to boost the 200-watt drive power to 3 to 4 kw. Output isolation was also provided to prevent variations in the experimental load from affecting tube operation.

#### Experimental Procedure

Five fully instrumented tests were conducted with the Crystallon-R heat exchanger at power levels of 0.9, 1.3, 2.0, 2.5, and 2.9 kilowatts, using the Amplitron power source. The air-flow rate varied between 21 and 23 cu ft per min. Additional fully instrumented tests were carried out on both the Niafrax and Crystallon-R heat exchangers using a high-power klystron transmitter. These tests were carried out while awaiting the completion of the Amplitron power supply. Power inputs in this case ranged from 0.7 to 2.0 kilowatts continuous power.

#### Experimental Results

Figure 7 shows the working fluid temperature rise and heat exchanger wall temperatures for several power input levels using the Crystallon-R heat exchanger. For comparison between the theoretically predicted performance of the heat exchanger and the experimental results, Figure 8 shows the 0.9-kw case plotted with the wall temperature determined from the heat transfer analysis. As observed, quantitative agreement is fair except in the entrance region of the heat exchanger. It was theoretically predicted that, since the notch reduced the attenuation area, maximum power dissipation in the heat exchanger would be at a point slightly downstream from the notch. It is possible, however, that the contact area between the stainless-steel feeder line flange and the inlet flange of the heat exchanger presented a very high electrical resistance to the propagating energy with an attendant high electric current density existing in this area. This would result in high energy dissipation and a very high temperature rise of the inlet flange structure which for theoretical purposes was assumed to attenuate no energy. It is possible, then, that sufficient heat was transferred to the heat exchanger

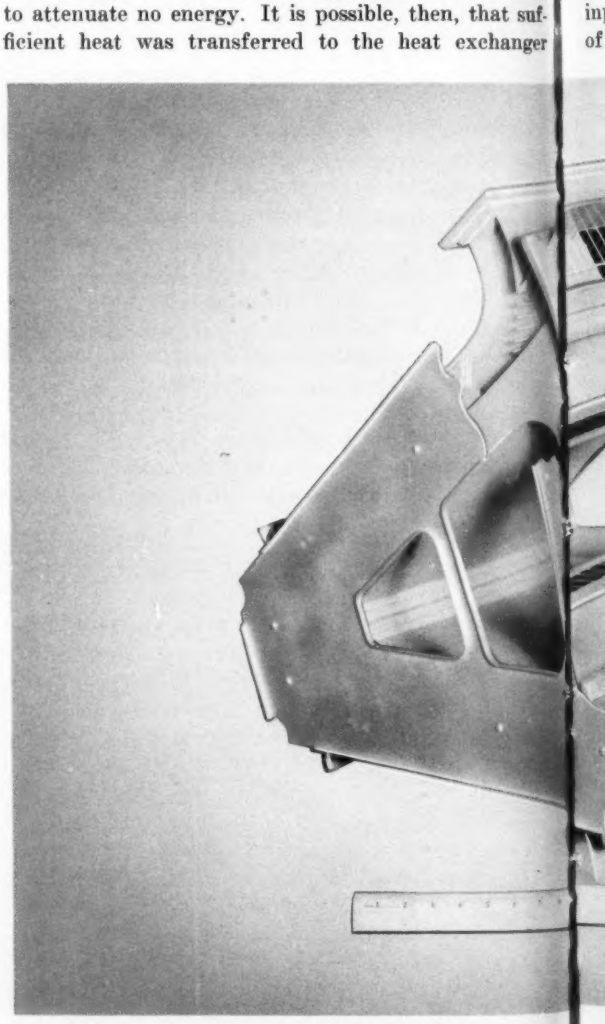

Figure 12. 76-Element Heat Exchanger

entrance to cause the highest wall temperature to occur at the entrance of the heat exchanger.

The over-all qualitative agreement between the analytical and experimental results was considered good in view of the complexity of the analysis and inherent experimental errors.

Since the attenuation characteristics of the heat exchanger are such that all the input microwave power is converted into heat, the heat unaccounted for by the air temperature rise must have been lost to the surroundings and to parts of the test structure outside the heat exchanger proper. Any failure to achieve a heat balance on the heat exchanger can be attributed only to experimental difficulties inherent in heat transfer measurements. The results of a heat balance analysis for the test conditions are presented in Figure 9. The heat unaccounted for by the air stream plus ambient losses and reflected power (absorbed upstream of the heat exchanger) account for 85 per cent of the input power at 0.9 kw power input and 72 per cent of the input power at 2.9 kw power input. This is reasonable in that ambient and reflected power losses increase with power input.

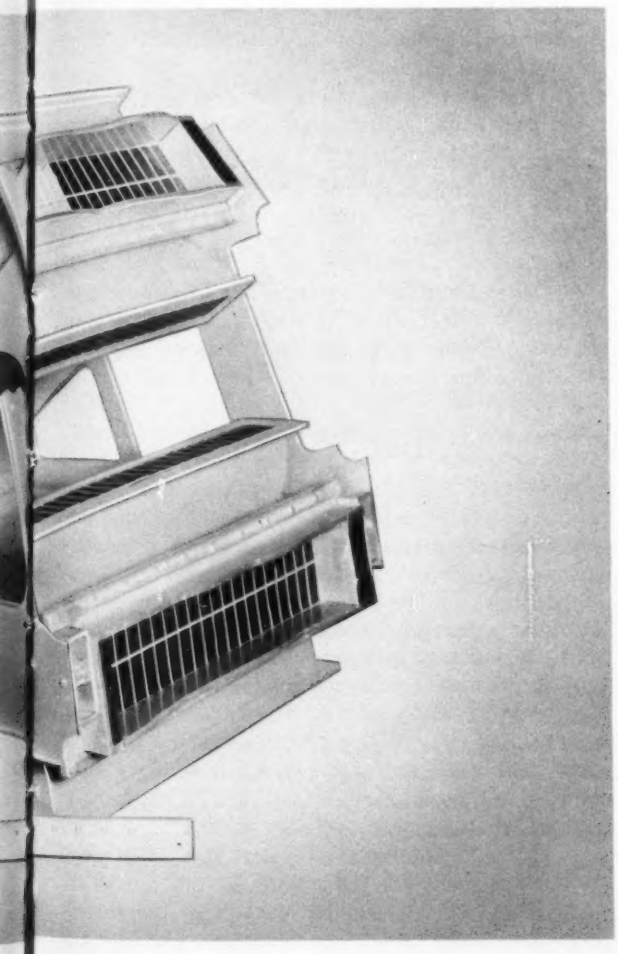

Figure 10 illustrates the temperature response of the Niafrax heat exchanger to power levels of 0.8 and 1.0 kilowatt. The klystron transmitter was used as the power source for these tests. Air temperature response is not listed for the 0.8 kw case because of instrumentation difficulties.

Electrical measurements for the test program entailed the determination of the power level at which waveguide arcing occurred, maximum heat exchanger VSWR, and the power attenuation capability of the heat exchanger.

For the Crystallon-R heat exchanger, arcing occurred at the 2.8-kw power level and increased in severity up to 3.0 kw. When arcing did occur, the arc remained close to the notched end of the center resistance strip. At 3.0 kw, the arc was maintained for several minutes before any disintegration of the heat exchanger was observed. The power-handling capability of the Crystallon-R model can be set under these test conditions at just under 3 kw. It is pointed out that working fluid pressure was slightly above atmospheric. Higher pressure levels would have prevented this arcing.

Another effect observed during the tests was that, at power levels in excess of 2.0 kw, expansion of the bolts fastening the heat exchanger to the stainless-steel feeder line allowed the heat exchanger and feeder line flanges to loosen. The increased electrical resistance to the transmission of microwave energy resulted in erratic arcing at the flange junctions. This permitted much higher energy dissipation and an associated temperature rise in the flanges than had been anticipated. The flange resistance can be reduced by the use of expansion bolts designed to ensure a tight junction between the flanges for the power levels of interest.

At power levels up to 3 kw, with arcing between the walls and center resistance strip, the VSWR remained under 1.5. The power attenuation of the Crystallon-R model was over 50 db for all power levels.

No arcing was observed on the Niafrax heat exchanger at power levels up to 2 kw, although arcing did occur at power levels between 2.5 and 3 kw. As with the Crystallon-R model, a tight coupling between the heat exchanger flange and stainless-steel feeder line flange could not be maintained because of expansion of the flange bolts. It is uncertain how the ionization due to sparking at the flange influenced the breakdown level in the area between the horizontal strips. In at least one case, complete breakdown did apparently originate at the flange, since this arc traveled back into the RF generator waveguide system and operated a photoelectric cell arc-protection circuit. Occasionally, arcs originating in the area near the flange were observed traveling along the surfaces

of the side walls. It is not known whether these arcs were surface discharges on the silicon carbide or breakdowns in small cracks in the material. With more sophisticated flange design and again, with a higher working fluid pressure level, this arcing can be prevented.

The VSWR remained under 1.5 and power attenuation remained greater than 47 db for all tests on the Niafrax heat exchanger. Higher working fluid pressures were not used on these tests because achieving the very high wall temperatures was an important aspect of the test program. Since available power was limited to 3 to 5 kw, higher pressure levels would have been accompanied by higher working fluid flow rates and consequently lower heat exchanger wall temperatures.

## Design Example

To illustrate the application of the analytical studies, the design procedure for selecting a heat exchanger of arbitrary power dissipation is explained.

The parameters to be determined in the analysis are: wall temperature distribution, working fluid temperature rise, total heat transfer surface area, Reynolds number, heat exchanger volume, and heat exchanger weight.

A design is initiated by selecting a power transmission frequency, f, which fixes the wavelength ratio, $\lambda_g/\lambda$, and the interior cross-sectional dimensions of the heat exchanger. For instance, if C-band energy is used, $\lambda_g/\lambda$ would be 1.1871 and the interior cross-sectional dimensions would be 1.872 by 0.872 in. The center-strip thickness can be taken as 0.125 in. Selection of this parameter is somewhat arbitrary. However, both theory and experimentation indicate this value to be a fair compromise between increasing the attenuation and decreasing the working fluid pressure drop. The number of incremental elements can be taken as 20. Increasing the number of increments beyond this would not contribute significantly to the accuracy of the finite differences analysis and would substantially increase the solution time. Using 2 for $\epsilon$, the tolerance of error between incremental element temperature balances, will provide sufficient accuracy. The heat exchanger material fixes the resistivity, thermal conductivity, and density. For a given resistivity, transmission frequency, and number of horizontal strips, n, the length of the heat exchanger is determined. This over-all length, L, then fixes the length of each increment, $\Delta X$ (equal to L/m), and the length of the inlet matching notch, $\Sigma$. The remaining parameters are determined from the application of the heat exchanger.

For example, consider the closed-cycle gas-turbine flow diagram in Figure 11. The full-scale heat exchanger for this application would be comprised of a bundle of waveguides or heat exchanger elements (100, for example). The mass flow rate of working fluid per element would then be W/100; initial working fluid temperature would be that existing from the exit of the regenerator. The specific heat $C_p$, would depend on the type of working fluid; initial working fluid pressure would depend on the pressure ratio of the compressor, the compressor inlet pressure, and the pressure drop through the regenerator. The energy, $P_o$, to be transferred per unit element would depend on the heat input to the engine. If 3000 Btu/sec heat input were necessary, the energy transferred per heat exchanger element would be 30 Btu/sec.

Substituting these parameters into Equations A-3, A-4, A-5, and A-6 of the accompanying heat transfer analysis and performing the indicated operations yields the following:

(1) Pressure drop of the working fluid,
(2) Weight of the heat exchanger, and
(3) Maximum heat exchanger wall and working fluid temperature rises along with their temperature distributions along the length of the heat exchanger.

With these parameters, the acceptability of the design can be readily evaluated.

It may be necessary to investigate several different bundle groupings before acceptable performance and weight are attained. However, sound judgment and rough heat transfer calculations tend to minimize the bundle groupings that must be examined.

Figure 12 illustrates a configuration of 76 individual elements designed for use in a 2100-shp closed-cycle gas turbine. The theoretical power transfer capability of this device is 3870 Btu/sec. This design was essentially based on the procedure outlined above.

## Conclusions

The basic heat transfer and microwave attenuation characteristics have been presented for several small experimental heat exchanger models. The experimental results indicated that the theoretical equations approximately predict the heat exchanger operating temperatures. In the course of the experiments, several material and fabrication problems were uncovered. These problems point out the need for extensive research and development in these techniques before a reliable microwave heat exchanger can be developed. Enough information has been obtained from this effort, however, to predict with confidence that the next heat exchanger development program will produce a reliable operating device.

Although this study program was carried out as part of a military system effort, commercial applications are conceivable. For example, an airship could be jet-stabilized in space through small open-cycle turbines utilizing microwave energy beamed from the ground as a heat source. The airship would house

television transmitting equipment to broadcast over a several hundred mile radius in the same manner as airplanes presently being used as television relay stations.

Another application is ground-to-ground wireless transmission of power. Raytheon Company is currently preparing a proposal for a short-range (approximately 1500 feet) ground-to-ground demonstration system including power transmitter, transmitting and receiving antenna systems, heat exchanger and turbine, electric generator, and load. The program is tailored toward modifying a production-type gas turbine of the order of 20 kw to operate on microwave energy. The combustion chamber would be replaced by a microwave heat exchanger. The current choice for the power generator is a 20-kw CW klystron transmitter operating at X-band. Transmitting and receiving antennas present many design problems and would be the subject of first studies in this program. Achieving an economical transmission efficiency depends strongly on the solution of ground reflection and focusing problems.

The microwave heat exchanger also can be used as a small light-weight load for very high power pulse or CW signals. In this application the heat output would be rejected to the ambient.

## HEAT TRANSFER ANALYSIS FOR A PARALLEL-FLOW HEAT EXCHANGER

A typical parallel-flow type heat exchanger is illustrated in Figure 2. Consider this heat exchanger to be composed of a series of incremental volumes, each of length $\Delta X$, as shown in Figure 13a.

If it is assumed that:

1) The heat exchanger (and therefore the incremental element) is perfectly insulated on its external surfaces; i.e., no heat losses to the environment,

2) All conditions in each channel are identical: the amount of heat generated, amount of air flow, etc.,

3) Heat is generated uniformly on all inside surfaces of each section of incremental volume,

4) The temperature throughout the material of each section of incremental volume is uniform,

5) No heat is conducted in the fluid stream itself,

6) There are no air-temperature gradients in the Y-Z plane,

7) The electrical resistivity of the material is constant, and

8) Steady-state conditions exist,

it is then possible to create a simplified two-dimensional model of the heat transfer interaction between heat exchanger surface and fluid flow as shown in Figure 13b. The rectangle *abed* represents the volume of material contained in the incremental volume shown in Figure 13a. It is at uniform temperature, given by $T\left(x + \frac{\Delta X}{2}\right)$. The rectangle *bcfe* represents the mass of air flowing through the incremental element and experiences a temperature rise from $T_X$ to $T_{(X + \Delta X)}$. The line *ad* represents all the external surface area of the incremental volume; there is no heat flow through this surface. The line *ab* represents the cross-sectional area for conduction in the $Y - Z$ plane at X, and the line *de* the cross-sectional area for conduction in the $Y - Z$ plane at $X + \Delta X$. The line *eb* represents all the internal surface area in the elemental volume for convection of heat to the air. Again, the heat is generated uniformly in the section *abed*. Utilizing a simple energy balance for the element and the fact that conditions are at steady state, it follows that:

$$q_{in} + q_{gen} = q_{out} + q_{conv}. \qquad \text{(A-1)}$$

It also follows that the heat convected to the air is proportional to the temperature rise experienced by the air, or:

$$q_{conv} = f(\Delta T_{fluid}). \qquad \text{(A-2)}$$

Then for each incremental element taken there are two equations describing the pertinent conditions.

With the simplified model of the incremental volume described above, the heat exchanger can be now represented as shown in Figure 14 where it has been divided into $m$ increments, each $\Delta X$ long. Although it does not show in this model, it must be remembered that because of the notch in the horizontal strips, the cross-sectional areas and heat transfer surface areas will vary from element to element for the length of the notch, $\Sigma$. In order to provide a proper electrical match, this notch must be at least one waveguide wavelength long. In order to simplify the analysis, it was specified that the length be made equal to the next multiple of $\Delta X$ that was larger than the minimum required for electrical matching. For example, if the length required electrically were 1.83 inches and if $\Delta X$ were 0.5 inch, then the length, $\Sigma$, would be specified as $4\Delta X$, or 2.0 inches.

As was previously stated, there are two equations for each incremental section: one resulting from a heat balance of the waveguide material, and the other from a heat balance of the air.

For an $r$*th* element, which includes elements 2 through $m - 1$, Equation A-1 (the heat balance for the element) can be written as:

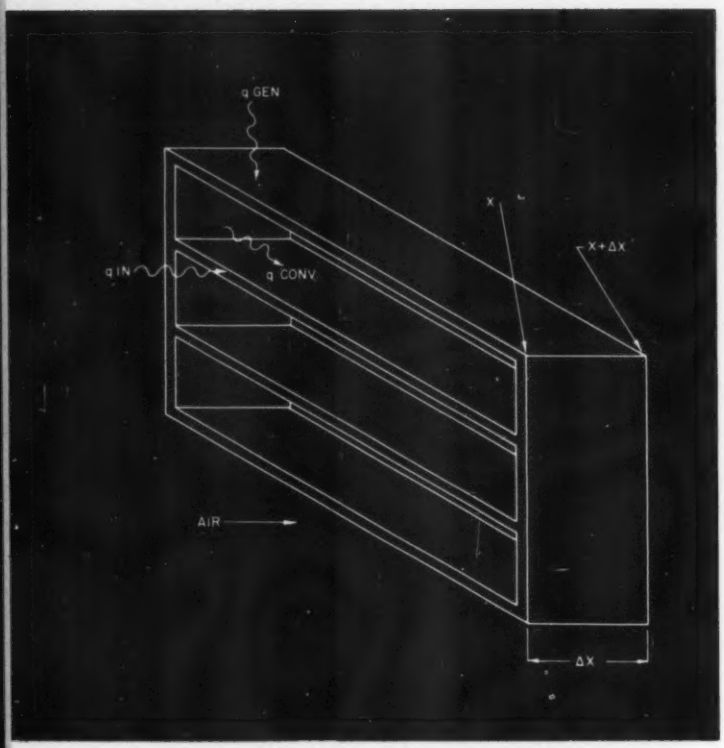


Figure 13a. Typical Incremental Element

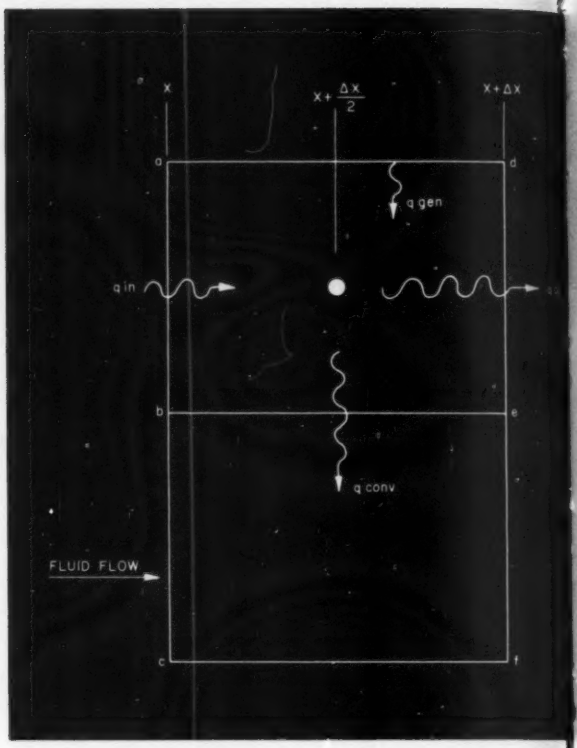


Figure 13b. Simplified Two-Dimensional Model

$$q_r = \left[P_{D_r} - P_{D_{(r-1)}}\right] - \left[\frac{k_w A_{c_{(r-1)}}}{\Delta X} + \frac{k_w A_{c_r}}{\Delta X} + h_r S_r\right] T_{(r-1)} + \left[\frac{k_w A_{c_r}}{\Delta X}\right] T_{(r-1/2)} + \left[\frac{h_r S_r}{2}\right] T_{(r-1)} + \left[\frac{h_r S_r}{2}\right] T_r = 0. \quad \text{(A-3)}$$

Equation A-3 is general for all material elements except the first and the m*th*. For the first element of material, there is no heat conducted into the element, $q_{in}$, and Equation A-3 therefore becomes:

$$q_1 = P_{D_1} + \left[\frac{k_w A_{c_1}}{\Delta X}\right] T_{3/2} - \left[\frac{k_w A_{c_1}}{\Delta X} + h_1 S_1\right] T_{1/2} + \left[\frac{h_1 S_1}{2}\right] T_1 + \left[\frac{h_1 S_1}{2}\right] T_o = 0. \quad \text{(A-4)}$$

For the m*th* element of material, there is no heat conducted out of the section, $q_{out}$, and Equation A-3 becomes:

$$q_m = \left[P_{D_m} - P_{D_{(m-1)}}\right] - \left[\frac{k_w A_{c_{(m-1)}}}{\Delta X} + h_m S_m\right] \frac{T_{2m-1}}{2} + \left[\frac{k_w A_{c_{(m-1)}}}{\Delta X}\right] \frac{T_{2m-3}}{2} + \left[\frac{h_m S_m}{2}\right] T_m + \left[\frac{h_m S_m}{2}\right] T_{m-1} = 0. \quad \text{(A-5)}$$

Equation A-2 (the heat balance on the fluid) is essentially the same for all elements and can be taken as:

$$q(r)_{air} = (h_r S_r)\, T_{r-1/2} - \frac{h_r S_r}{2} + WC_p T_r - \frac{h_r S_r}{2} - WC_p T_{r-1}. \quad \text{(A-6)}$$

The heat generated in an incremental volume $\Delta X$ of the heat exchanger $(P_{D_r} - P_{D_{r-1}})$ can be derived as follows. The rate of change of power as a function of heat exchanger length is:

$$\frac{dP}{dX} = 2\alpha P.$$

The solution for P is:

$$P = P_o e^{-2\int \alpha\, dx},$$

where $\alpha$ is the attenuation constant, and $P_o$ is the entering power level. By induction, the total heat generated in the waveguide as a function of X can be expressed as:

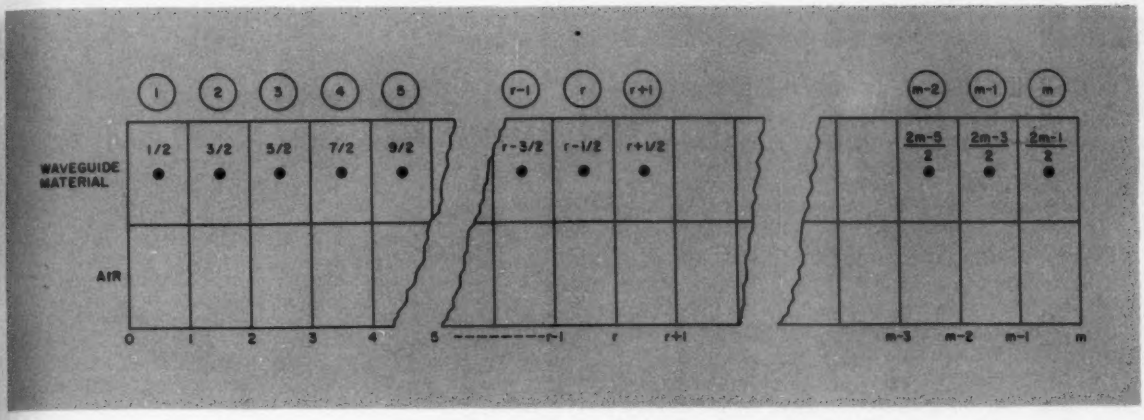


**Figure 14. Analytical Model of Heat Exchanger**

$$P_D = P_o - P = P_o\,(1 - e^{-2\int \alpha\, dx}). \qquad \text{(A-7)}$$

$\alpha$ is defined by three terms: first, when there are no horizontal strips ($\alpha_o$); second, when there are an arbitrary number of strips ($\alpha_b'$); and third, when during the transition region ($\alpha_t$). The attenuation constants $\alpha_o$, $\alpha_b'$, and $\alpha_t$ are given by:

$$\alpha_o = 7.5\sqrt{\rho}\sqrt{f}\,\frac{\lambda_g}{\lambda}\left[0.002222\left(\frac{1}{b}\right) + \left(\frac{1}{a^3}\right)\left(\frac{1}{f^2}\right)\right]. \qquad \text{(A-8)}$$

$$\alpha_b' = 7.5\sqrt{\rho}\sqrt{f}\,\frac{\lambda_g}{\lambda}\left[0.002222\left(\frac{1}{b}\right) + \left(\frac{.1}{a^3}\right)\left(\frac{1}{f^2}\right)\right]. \qquad \text{(A-9)}$$

$$\alpha_t(X) = \alpha_o + \frac{\alpha_b' - \alpha_o}{\Sigma}\,X. \qquad \text{(A-10)}$$

Note that $\alpha_o$ and $\alpha_b'$ are not functions of X. Using Equation A-7 and performing the indicated operation, the following expressions for $P_{D_r}$ are obtained:

$$P_{D_r} = P_o\,[1 - e^{-2(\alpha_o r\Delta X + \frac{\alpha_b' - \alpha_o}{2\Sigma} r^2\Delta X^2)}],$$

and for $r\Delta X \leq \Sigma$,

$$P_{D_r} = P_o\,[1 - e^{-2[(\alpha_o + \frac{\alpha_b' - \alpha_o}{2})\Sigma + \alpha_b'(r\Delta X - \Sigma)]}].$$

Since the heat transfer coefficient is a function of temperature, it is normal to express it as:

$$h(t) = K(a_o + a_1 T_{fluid} + a_2 T^2_{fluid} + a_3 T^3_{fluid}), \qquad \text{(A-11)}$$

where K represents physical constants not dependent on temperature. The constants $a_0 \ldots a_3$ are determined by plotting the physical constants dependent on temperature as a function of temperature, and by

**Table 2. Glossary of Symbols**

| | |
|---|---|
| A | Cross-sectional area for heat conduction ($ft^2$) |
| a | Inside waveguide width (ft) |
| B | Entrance loss coefficient |
| b | Inside waveguide height (ft) |
| b′ | Distance between lossy strips (ft) |
| $C_p$ | Specific heat of air (Btu/16°F) |
| D | Equivalent diameter (ft) |
| d | Density of waveguide material ($lb/ft^3$) |
| f | Frequency of microwave propagation (kmc/sec) |
| h | Convective heat transfer coefficient (Btu/hr-$ft^2$-°F) |
| $k_w$ | Thermal conductivity of waveguide material (Btu-ft/hr-$ft^2$-°F) |
| L | Length of heat exchanger (ft) |
| m | No. of increments |
| N | No. of unit cells used to comprise heat exchanger |
| n | No. of horizontal lossy strips |
| P | Unattenuated power in waveguide (Btu/sec) |
| $P_D$ | Heat generated in waveguide as function of distance along waveguide (Btu/sec) |
| $P_o$ | Initial incident power into waveguide (Btu/sec) |
| r | Numerical index |
| S | Surface area for heat convection ($ft^2$) |
| $R_s$ | Surface resistance (ohm/square) |
| T | Heat exchanger wall temperature (°F) |
| $t_w$ | Thickness of waveguide walls (ft) |
| $t_s$ | Thickness of lossy strip (ft) |
| W | Mass flow rate of air per unit cell (lbs/sec) |
| X | Distance along the length of the waveguide (ft) |
| Σ | Length of taper or notch (ft) |
| ρ | Electrical resistivity of waveguide material (ohm-cm) |
| p | Pressure drop in water (psi) |
| α | Attenuation constant (nepers/unit length) |
| $\alpha_g$ | Attenuation constant in waveguide (nepers/unit length) |
| σ | Electrical conductivity $(\text{ohm-meter})^{-1}$ |
| λ | Wavelength in unbounded medium (cm) |
| $\lambda_c$ | Cutoff wavelength (cm) |
| $\lambda_g$ | Wavelength in waveguide (cm) |
| μ | Magnetic permeability ($\mu_o = 4\times10^{-7}$ Weber/volt-meter for free space and non-ferrous metals) |
| ε | Dielectric constant ($\epsilon_o = \frac{1}{36}\times10^{-9}$ Coulomb/volt-meter for free space and metals) |

then selecting the constants $a_0 \ldots a_3$ so that the expression in parentheses of Equation A-11 will fit the curve.

Since the temperature change encountered over a distance, $\Delta X$, could be large, a mean heat transfer coefficient should be used over each element.

Then: $$h_r = h_{mean}, \qquad (A\text{-}12)$$

where the mean coefficient is defined by:

$$h_{mean}\,(T_r \Delta T_{r-1}) = \int_{T_{r-1}}^{T_r} h\,(T)\,dT. \qquad (A\text{-}13)$$

Because the determination of the heat transfer coefficients depends upon the air temperature distribution, and since this is one of the quantities of interest, an iterative solution to the heat transfer equations must be used. In solving the equations, an initial air temperature profile is assumed to vary linearly between $T_o$ and $T_m$ ($T_m$ is implicitly specified by $P_o$ and W). Corresponding values for $h_r$ are then calculated from Equation A-13, and substituted into Equations A-3, A-4, A-5, and A-6. When this set of 2m simultaneous equations are solved, a new air temperature profile is specified. New values of $h_r$ are then computed and the process repeated until satisfactory heat balances are attained. Solutions to the equations can be readily carried out on an IBM 704 computer. The numerical technique deemed most suitable for solving these equations is the method of Gaussian Elimination.

A standard correlation was used to obtain pressure drop data:

$$\Delta P = \left(\frac{4f\rho L}{D} + K\right)\frac{w^2}{2g\rho a A^2}. \qquad (A\text{-}14)$$

In order to obtain a ratio of pressure drop to initial pressure, Equation A-14 is divided by $P_o$. Rewriting Equation A-14 in simpler terms and expressing K numerically to account for inlet and exit losses, the pressure drop ratio is:

$$\frac{\Delta P}{P_o} = \left[\frac{2f\rho L\,(a+b')}{ab'} + 0.4\right]\frac{w^2}{2g\rho_{avg}(n+1)^2 P_o a^2 b'^2}. \qquad (A\text{-}15)$$


## Acknowledgement

The engineering work described in this article was performed at the Surface Radar and Navigation Operations Engineering Activity of the Equipment Division. Contributions to the work were made by Edward L. Green, George M. Hamm, and Melvin W. Tracy, as well as the author.


## INVENTIONS

Congratulations to the following persons for their valuable contribution to Raytheon's portfolio of inventions:

| *Name* | *Field of Invention* |
|---|---|
| Louis H. Schall | Microwave Cooker |
| Louis H. Schall | Microwave Oven Feed & Adaption System |
| Gerhard A. Flodberg | Unit Assembly Fixture |
| Paul W. Stutsman | Cold Cathode Sensitive Trigger Tube |
| Charles R. Wexler | Frequency Modulation Detector |
| Lennart W. Bjork | Window Assembly for Ridge Guide |
| Edward C. Dench | Hydraulic Tuning of Magnetrons |
| Harry F. Chapell | M-BWO's Efficiency Device |
| Harold R. Shurtleff, George E. Burdick, Vaughn T. Judd | Welding Machine |
| Louis T. Jansen | Cathode Ray Tube |
| Robert E. Edwards | Rotary Tuner |
| Ray C. Ellis, Jr. | Silicon Carbide Coating |
| John M. Osepchuk | TPOM with Regenerative Feedback |
| Paul E. Mills | Emissive Coating Binder |
| Raymond P. Tuinila, Thomas J. Griffin | Precision Ultra-Sonic Deburring |
| Richard P. Curtis | Anti-Collision Plotter |
| Herbert Single, Leonard Emerson | Depth Sounder |
| John N. Beebe | Automatic Synchronizer |
| Richard H. Dutton | Bright Display Symbol Generator |
| George Rupprecht | Polarizer for Infra Red Light |
| Seymour Cohen | Tunnel Diode Power Supply |
| Allen H. Smith | Coating Method |
| Wilhelm Rindner | Exact Positioning Method |
| Max Michelson | Ferrite Circulator |
| Frank Zawada, Malven Arnum | Network Strap Transformer |
| William M. Murphy, Jr. | Doppler Fuzing System |
| Robert A. Fryklund | Infra-Red-Critical-Course Indicator |
| Robert M. Chute | Display System |
| John D. Harmer | Feedthrough Nulling System |
| Arthur B. Slater | Compression Systems |
| William M. Hall | MTI Scan Modulation Elimination |
| J. Francis Ahearn | Insulated Conductor |

## PAPERS & PUBLICATIONS

R. HARPER, R. HERGENROTHER, R. McC. UNGER, "A Single-Voltage-Control Electrostatic-Focus Backward Wave Oscillator for X-Band Operation," presented at the Professional Group on Electron Devices, Washington, D.C., Oct. 27-28, 1960.

This paper describes an X-band backward wave oscillator using the electrostatic focus principle applied to an interdigital line. The tube operates over the frequency range of 8.5 to 9.6 kmc with a minimum power output of 20 mw and can be voltage-tuned by altering a single electrode voltage. The tube is of metal and ceramic construction and has a waveguide output projecting from its side which may be used for supporting the tube. The use of electrostatic focus has permitted a weight reduction of 75 per cent over a corresponding magnetic focus tube, resulting in a net tube weight of 1.5 lbs. The design of the interdigital line is described, and performance curves for the tube are presented.

J. R. PATEL, A. R. CHAUDHURI, "The Dependence of the Mechanical Properties of Dislocation-Free Germanium on the Electronic Properties," presented at the Meeting of the American Institute of Mining, Metallurgical and Petroleum Engineers, Philadelphia, Pa., Oct. 17-21, 1960.

It has been found possible to relate the deformation characteristics of germanium crystals to certain electronic properties of the crystals. The effects of heavy doping with an n-type donor or a p-type acceptor element on the maximum stress reached during the tensile deformation of dislocation-free germanium have been reported previously,[1] and are due to the change in the velocity of dislocations between the doped and undoped germanium crystals.

The Fermi level is also a function of the temperature and the type of doping of the crystals. From measurements of the concentration dependence of either the maximum stress or the velocity at various temperatures, it has been found that information can be obtained on the intrinsic carrier concentration as a function of temperature, on the displacement of the Fermi level from the center of the energy gap, and on the position of the vacancy energy level. These determinations from the mechanical measurements are in good agreement with the direct electrical measurements of these parameters.

[1] A. R. Chaudhuri and J. R. Patel, Bull. Amer. Phys. Soc. Series II, *5*, 264 (1960).

J. BROWNSON, R. SAPHIR, "Some Statistics of Silicon Crystal Doping," presented at the Electrochemical Society Meeting, Houston, Texas, Oct. 11, 1960.

The first section of this paper deals with the impurity distribution among N-type silicon crystals and the sources of impurity variation. Of 828 doped crystals, an essentially normal distribution was found. The sources of variation, in order of importance, are shown to be the dopant, raw silicon, process variation, crucible variation, and measurement variation.

The second section deals with graphical data necessary to estimate actual yields in relation to parameters of resistivity variation, desired resistivity bandwidth, and segregation coefficients. In summary, control chart data is presented illustrating how actual values of yield mean and distribution spread compare with predicted values.

L. G. RUBIN, D. L. PHIPPS, J. WELTS, "Punched Card Data Acquisition as Applied to the Measurement of Basic Semiconductor Properties," presented at the Session on Instrumentation Research, Meeting of the Instrument Society of America, New York, N.Y., Sept. 27, 1960.

The measurement of the resistivity, Hall effect, and magneto-resistance of semiconductors as a function of temperatures constitutes an important but time-consuming phase of semiconductor technology. For this reason, an apparatus has been constructed to perform the task automatically over the temperature range from 1°K to at least 800°K. An IBM 526 summary punch, used in conjunction with a six-channel recorder and an analog-digital converter, makes possible the acquisition of the pertinent data in the form of punched cards. An IBM 650 computer is subsequently employed to reduce the data into its desired form.

## TECHNICAL PUBLICATIONS PANEL

| | |
|---|---|
| Chairman | O. T. FUNDINGSLAND |
| Secretary | M. A. WALKER |
| Commercial Apparatus and Systems Division | R. P. CURTIS |
| Industrial Components Division | C. CARRUTHERS |
| International Services | T. J. KELLY |
| Law Department | E. J. GORN |
| Missile Systems Division | J. W. BRODERICK, JR. |
| Microwave and Power Tube Division | W. W. TEICH |
| Public Relations | G. G. BARKER |
| Receiving Tube Operations | V. K. ULRICH |
| Research Division | H. R. BOYD |
| Semiconductor Division | F. M. DUKAT<br>D. RUBINFIEN |
| Airborne Electronic Equipment Operations | E. HADGE |
| Communications and Data Processing Operations | G. PARTRIDGE |
| Santa Barbara Operations | (to be named) |
| Submarine Signal Operations | L. BATCHELDER |
| Surface Radar and Navigation Operations | W. M. HALL |
| Raytheon Canada | J. KADISH |

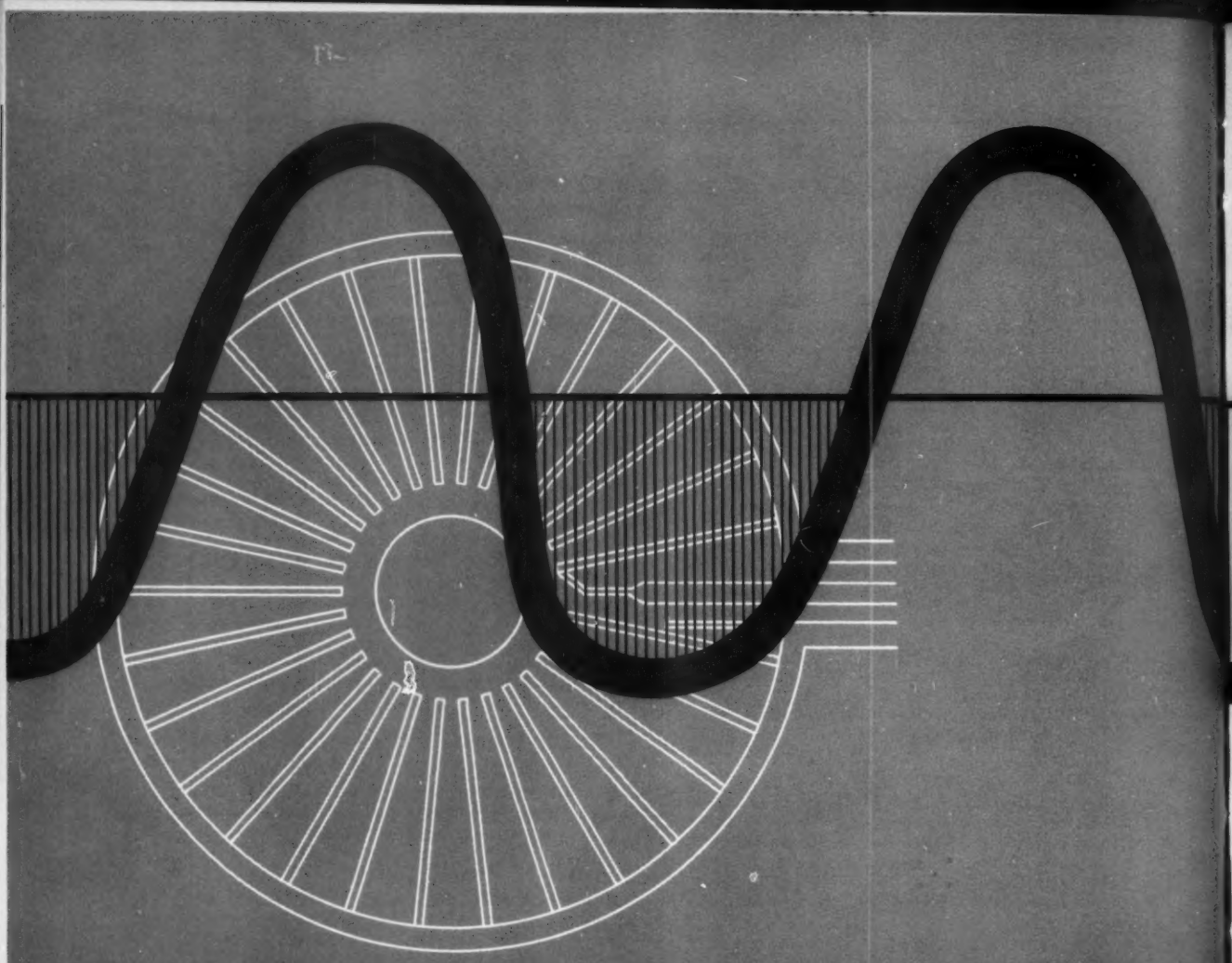

A HIGH POWER MICROWAVE ENERGY

# RECTIFIER

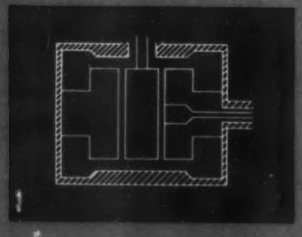

**JOHN F. SKOWRON** *is a Project Section Head in the High Power Tube Laboratory, Microwave and Power Tube Division. He joined Raytheon in 1949 and has worked on a series of high-power CW jamming magnetrons, a medium-power pulsed X-band tube for fire control equipment, the Stabilotron, and a special high-power UHF magnetron. Several of his innovations in magnetron design have been patented by Raytheon. Since 1956 his major concern has been the development of high-power traveling wave tubes. Mr. Skowron received his B.S. and M.S. degrees in Electrical Engineering from the University of Michigan.*

**JAMES B. THOMAS** *is a Research Physicist in the High Power Tube Laboratory, Microwave and Power Tube Division. Prior to joining Raytheon in 1955, he was a teaching assistant at MIT while continuing his graduate studies in solid state physics. At Raytheon he has been engaged in space-charge research studies, and a study of factors affecting cold cathode starting of Amplitrons. He is presently studying high-power microwave rectification devices. Mr. Thomas received his B.S. degree in Physics from MIT.*

In recent years the use of microwave generators for the wireless transmission of sizable amounts of power has come closer to reality. This possibility has intrigued microwave engineers since it promises a means of supplying power to remote locations where conventional transmission methods are not suitable.

The problems connected with such a development are difficult and challenging. Not the least of these problems is the necessity for a device to convert the microwave power to either direct current or alternating current at a voltage level which is suitable for operation of the using equipment.

At the Microwave and Power Tube Division an investigation has been conducted with the ultimate objective of obtaining an efficient high-power microwave-to-DC conversion device. This article offers some possible approaches toward achieving such a device and presents the results of an initial experiment using one of these approaches.

The usual method of obtaining a DC signal from microwave energy has been by the use of crystal rectifiers. These, however, are useful only at milliwatt power levels. In converting kilowatts or megawatts of RF to DC, the power-handling capability assumes considerable importance as does the device's efficiency of conversion. It is logical, therefore, to concentrate on interaction methods similar to those of microwave electron tubes which have demonstrated the capabilities of handling high levels of power and of providing efficient interaction mechanisms.

In the microwave electron tube generator or amplifier, the conversion of DC to microwave energy is effected by imparting either kinetic or potential energy to an electron stream and then translating it into microwave energy. In the microwave converter we are interested in performing the reverse function. One device that functions in such a reverse manner is the linear accelerator. Here a stream of electrons is accelerated by a microwave signal which imparts energy to the stream; this energy is then released upon striking a target. The objective in a microwave converter is to change this energy into the form of a potential or voltage suitable for driving an external load. Generally speaking, the limitations that required the development of microwave tube principles, such as transit time and inter-electrode capacity, likewise apply to a converter.

The general principle of operation of a microwave energy converter can be illustrated by the specific case of a beam-type tube shown schematically in Figure 1. An electron gun accelerates a beam, which passes through a microwave interaction region, gains additional velocity, and then strikes a collector. The potential of the collector is depressed negatively by means of current through an external load. Ideally, if all electrons were accelerated equally by the microwave signal, the excess energy thus gained would be placed into the external load and the bias produced would just stop the beam, resulting in negligible dissipation at the collector. Needless to say, such an idealization would not be practically realized for several reasons. Due to space charge effects at the collector and related problems, it is not possible to stop the beam without any dissipation even if all

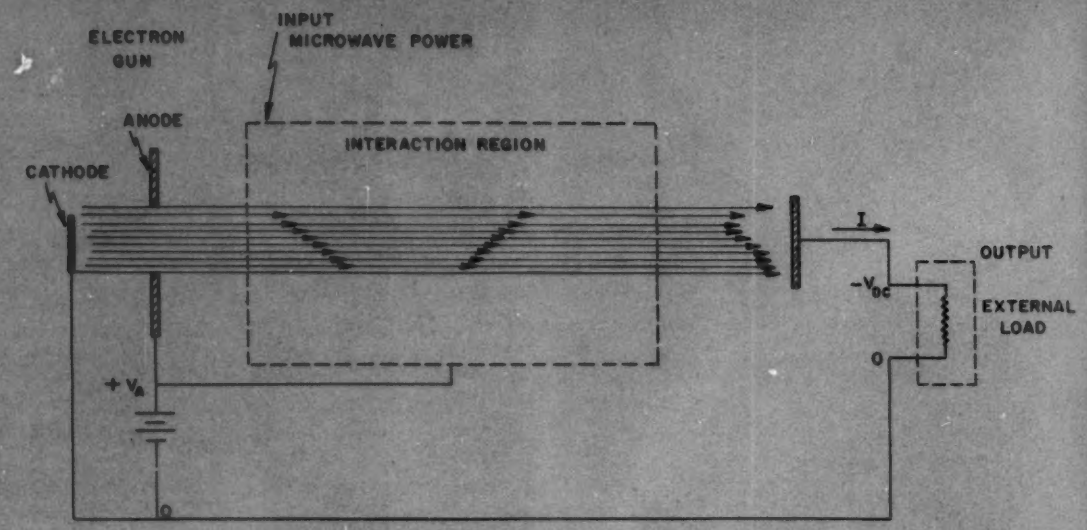


Figure 1. Beam-Type Microwave Energy Converter

electrons are equally accelerated. What is more important, however, is that the velocity spread inherent in linear beam interaction will not allow use of full bias to stop the fastest electrons. Consequently, one would expect that the efficiency would not be in excess of values typically obtained in linear beam amplifiers. It should be noted, however, that there is no "small signal" region of interaction in the usual sense since maximum signal is introduced into the front end of the tube. Interaction of this type might resemble that of a TWT in the region of saturation and beyond. An analysis of a device of this type would have to be done on a large-signal basis or experimentally. Neither type of analysis has ever been done.

To realize good efficiency, an interaction would be required in which the existing velocity spread is minimized or in which the electrons are tightly bunched. This requirement strongly suggests that crossed-field interaction would produce a higher efficiency than any of the other types of interaction. Among the crossed-field types of interaction which have been suggested are those involving velocity sorting by means of the magnetic field as well as cyclotron types. Since the high efficiencies demonstrated by magnetron- or Amplitron-type crossed-field devices suggest this type of interaction to be most promising, an initial experiment was conducted in this area.

Figure 2 shows the usual schematic anode voltage of a magnetron in rotating coordinates. The distance in the tangential direction of the rotating coordinates is plotted horizontally, and the anode voltage is plotted vertically. The shaded sections indicate the regions which are accessible to electrons. These regions are the parts of the RF cycle in which the electric field is retarding and in which the anode voltage exceeds the threshold potential. The threshold voltage, commonly called the Hartree voltage, depends on the magnetic field, the synchronous velocity and the dimensions, and is the voltage required for electrons to reach the anode while still remaining in synchronism with the traveling wave.

Although not shown in the diagram, the electron current generally peaks near the leading edge of the spoke where the RF potential is swinging negative. The voltage and current are so phased that the spoke looks like a generator to the RF circuit, thus building up or sustaining the RF wave. The DC voltage and current are so polarized that the magnetron looks like a load to its DC power supply.

Figure 3 shows a corresponding schematic for the condition under which microwave conversion would occur. Note that a large RF voltage relative to the Hartree potential is placed on the structure, and the nominal DC voltage on the anode is now negative with respect to the cathode. Electrons reach the anode in regions where the peak RF voltage exceeds the Hartree voltage plus the DC voltage. Note also that the spoke is positioned in regions of positive RF voltage in contrast to the negative part of the cycle, as in the preceding case. The voltage and current are thus phased so that the spoke looks like a load to the RF circuit rather than a generator. Since the electron flow is still directed from cathode to anode but the DC voltage has reversed polarity, the device now looks like a generator to the external circuit rather than a load. Conditions such as these should, therefore, fulfill the requirements of a microwave energy converter.

Because of the inherent complexity of analytical methods in crossed field problems, no attempt was made to predict the performance except in a qualitative fashion, and experimentation was conducted to

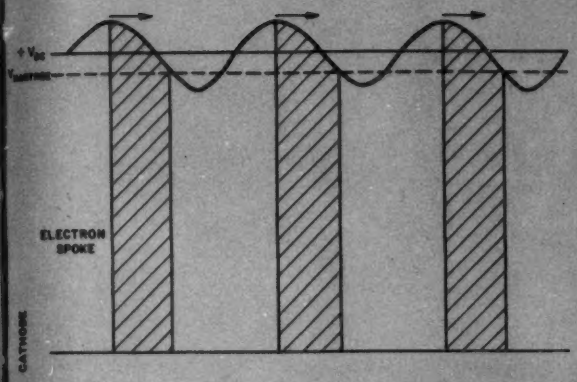


Figure 2. Anode Voltage and Position of Electron Spoke in the Magnetron

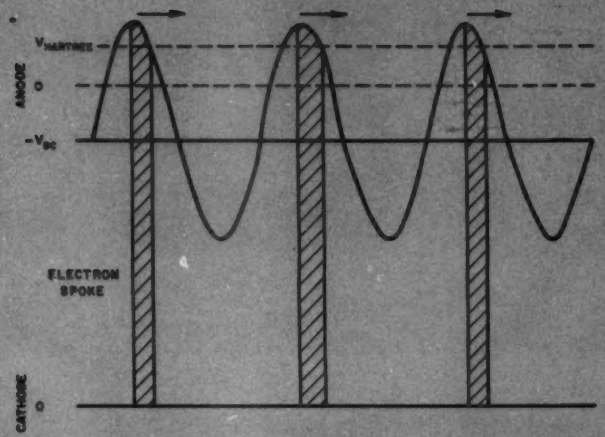


Figure 3. Anode Voltage and Position of Electron Spoke in the Microwave Energy Converter

establish feasibility. The parameters of interest in evaluating the behavior of the device are:

(1) The microwave input power which, together with circuit impedance, establishes the RF voltage level,

(2) The magnetic field which, with a given geometry, determines the Hartree voltage, and

(3) The DC load impedance which establishes the DC voltage for a given power.

Figure 4 shows the conventional magnetron performance chart plotted on DC voltage vs. current coordinates. The region of positive DC voltage is the region of operation of a magnetron and is illustrated by a typical operating line for a constant magnetic field (commonly called a gauss line). In contrast to this, the operating region of a converter would be in the negative area of the chart. A typical operating line would be along a diagonal extending toward the lower right from zero current and voltage.

In designing the experimental model several interesting considerations arose. One of these was that with a cathode which is generally positive with respect to the anode there was no need to have the usual end-shields on the cathode. Another consideration was that with a resonant structure, such as a re-entrant vane circuit, it would be desirable to couple the circuit very heavily to the external transmission line in order to minimize internal circuit losses. With heavy coupling the cold circuit would, of course, reflect back into the transmission line nearly 100 per cent of the incident power. With the rectifier in operation, presumably the electronic loading on the circuit would reduce the internal Q until, ideally, all of the incident power entered the rectifier and none was reflected. This would correspond to the 50 per cent coupling situation or a matched load under operating conditions.

In the course of the design, some question arose concerning the relative merits of $\pi$ mode operation versus pass band operation, on the grounds that $\pi$ mode operation would make the model less versatile. Since the structure is driven externally, mode separation as such is not of any consequence, and operation in the pass band would allow the investigation of several different circuit modes. In order to achieve the overcoupled condition for many modes, the structure was made nonre-entrant to exclude decoupled doublet modes. An unstrapped vane network was used to obtain a high-impedance circuit. Figure 5 is a drawing of the model showing a 29-vane network with isolation between front and rear. The frequency used was in the L-band region and was chosen mainly for convenience of related equipment. Pulsed operation was employed because of the existence of driver sources. The tube dimensions and parameters were chosen to allow test conditions having a low Hartree voltage and good separation between the Hull cutoff condition and Hartree voltage.

Some of the data that has been obtained with this tube is shown in the succeeding figures. All of the data shown is for the $\eta = 12$ mode number, the mode with 12 wavelengths along the network. The data for some of the other modes was very similar to that shown.

Note that the peak of power output occurs at higher magnetic fields and increases with higher input power levels, as one would expect. Note also the power output obtained at zero magnetic field. This is particularly evident in the data shown in Figure 6, which was taken with a load impedance of 2200 ohms. In this model the anode-cathode spacing was compara-

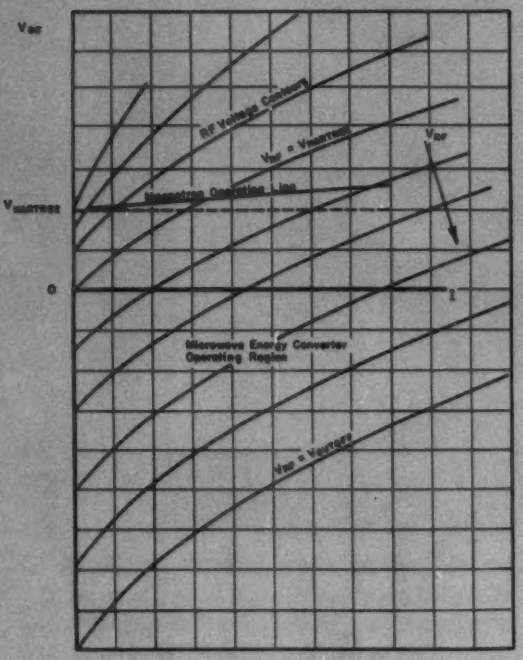


Figure 4. Crossed-Field Device Performance Chart

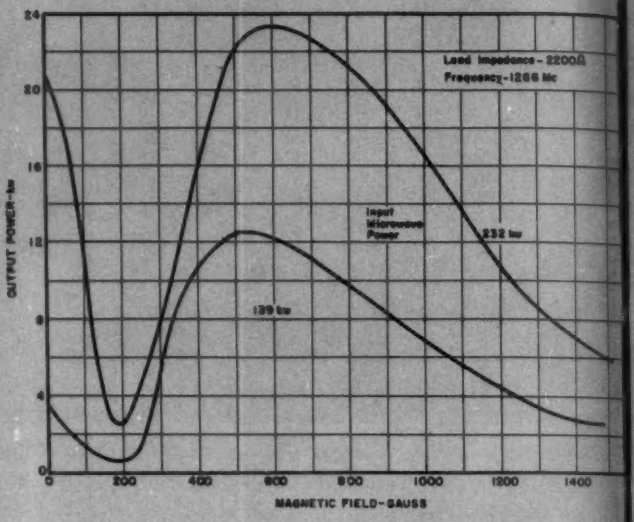


Figure 6. Microwave Energy Converter Data

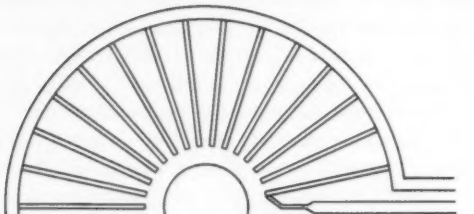



Figure 5. Schematic of Microwave Energy Converter

tively small while the RF voltage was comparatively large, especially at the 232-kw input level. It would appear that the RF voltage was sufficiently high to counteract some of the limitations imposed by the transit-time conditions. Generally, the appearance of sizable power at zero magnetic field occurred when drive level and load impedance were high. Calculations showed that the transit time was a relatively small fraction of a cycle under these conditions. For lower values of load impedance and for lower drive levels, the curves were similar but reduced in magnitude, and power at zero magnetic field was low relative to values at 500 or 600 gauss.

The dip in power output occurring at approximately 200 gauss is in the general region of the characteristic magnetic field, $B_o$, but not in the identical value as $B_o$. At higher magnetic fields synchronous conditions prevail whereas at low magnetic fields essentially a non-magnetic diode exists. Between these two conditions there should be a situation in which electrons leaving the cathode acquire tangential motion but not sufficiently soon enough to remain in favorable phase with the RF wave. This would result in unfavorable interaction and the drop in power output and efficiency at this point.

Cyclotron interaction was also observed in the form of a discontinuity in the power output characteristic in the region of about 450 gauss. This was found to shift slightly with power level. Several other slight discontinuities were also observed at the higher levels

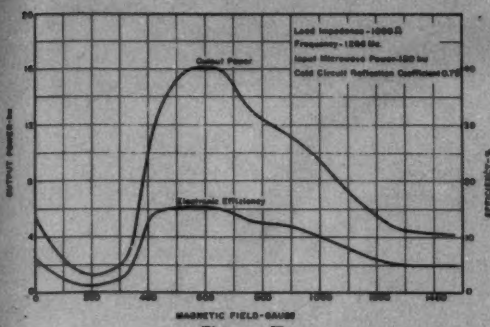


Figure 7.

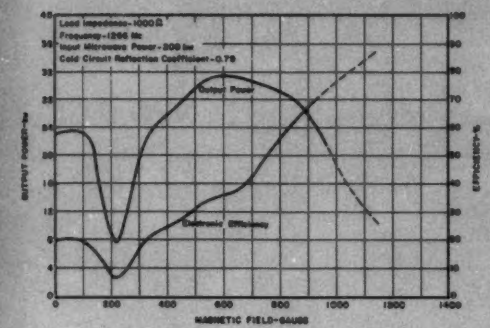


Figure 8.

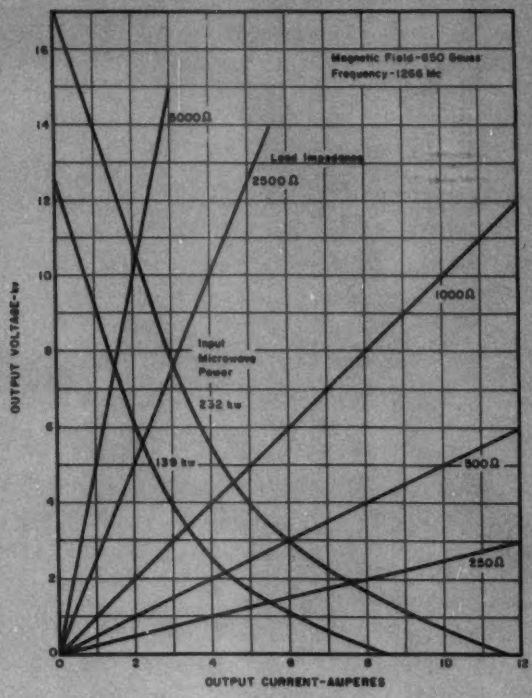


Figure 9.

Microwave Energy Converter Data

of power. No clear explanation of these discontinuities was found although interaction with space harmonics was suspected as a possible cause.

The efficiency of interaction is one of the important factors in a device such as this. The difference in interaction efficiency between the non-magnetic diode and the magnetic case is shown in Figure 7. Note that although the efficiency is higher at 600 gauss than at zero gauss, at this power level (120 kw) the efficiency is not especially high. Figure 8 taken at higher drive shows higher interaction efficiencies, in the 30 to 40 per cent region. The efficiency continues to rise with higher magnetic field but, due to the decline in power absorbed from the drive source, the measurement accuracy rapidly deteriorates, so that in this respect data beyond approximately 800 gauss is questionable. In regions where the electronic efficiency is quite high, the electronic conductance turns out to be quite low. In other words, the amount of power actually coupled to the electron stream is not high, with the result that most of the incident microwave energy is reflected back toward the source and does not enter the rectifier. The resultant total efficiency is, therefore, in the 10 to 15 per cent range. Improvement in total efficiency would evidently require the readjustment of converter parameters to more effectively load the external circuit while operating in the region of good electronic efficiency.

Figure 9 shows a performance chart at a single value of magnetic field. This essentially describes the sensitivity of the device to DC load conditions. Measured data coincides with intersections of the curves with the DC load lines. The extreme limits at zero volts and zero current are extrapolations based on estimates of limiting conditions. Constant efficiency contours would be hyperbolas with the efficiency broadly maximizing in the region of the 1000-ohm line.

All of the data presented here was obtained without the use of heater power on the cathode. Data with and without heater power was found to be substantially the same. It was thus possible to inject microwave power into one end of this device and obtain DC power at the other end without the use of any auxiliary power or voltages.

In summary, a microwave energy converter based upon magnetron interaction principles has been designed, built and tested. Data was obtained in the kilowatt range of power output, demonstrating the feasibility of this method for high power microwave conversion. With design improvements, over-all efficiencies in the 50 to 70 per cent range are believed to be possible since this is the efficiency range of magnetrons and Amplitrons, tubes which are also based on a crossed-field interaction. The same factors which determine the efficiency of magnetrons and Amplitrons similarly determine the efficiency of an energy converter. The design improvements would be in the areas of optimizing the design of the anode circuit, the coupling, the ratio of cathode to anode diameter, and the relative operating region.

# STATISTICAL ANALYSIS AS AN ENGINEERING TOOL

## PART 2

WE have seen that the properties of a normal distribution are such that we can describe the distribution completely by finding its two parameters; i.e., the mean and the standard deviation. (See ELECTRONIC PROGRESS, Sept.-Oct., 1960.) From these two parameters we can state by very simple calculations the limits within which any stated portion of the distribution lies. In order to make such statements, however, we must be sure that we are dealing with a normal population.

Many populations met in practice are normally distributed. This is particularly true for dimensions of mechanical parts at the point of manufacture. It is not necessarily true for mechanical parts which have been screened for dimension, or for parts which have come from different sources and have been mixed. In the first case we may be dealing with a selected part of a population, in the second with two or more populations. In addition to this sort of deviation from normality, we have populations which deviate from normality as manufactured. Many electrical characteristics are of this type. In a batch of transistors, the leakage current of 80 per cent of the population might be less than 2 microamperes while that of the remaining 20 per cent might range up to several hundred microamperes. Such a distribution is clearly not symmetrical, and therefore not normal. How can we tell what kind of population we are dealing with?

The usual first step in analysis of a population is to make a graphical picture of the distribution in the form of a frequency histogram. The frequency histogram is a bar chart in which the x axis is the range of measured values divided into equally spaced cells, and the y axis is the number of samples whose values fall into the cell range. For example, take the array of numbers in Table 1, which represents the weight gain from plating for a random sample of 40 parts. We first examine the table and find the largest and smallest values. The difference is the range, or 6.2 milligrams. If we divide this into 14 cells, each cell will be 0.5 mg. wide. We lay out our graph, and fill it in.

At the end we have a rather ragged histogram (Figure 1), but we can sketch in a bell-shaped envelope to the histogram which looks like a reasonable fit. The irregularities occur because we have only 40 measurements to divide among 14 cells, and we should not be surprised that some of the cells do not get their full quota.

The mean appears to be about 9.5. Suppose we repeat the operation using 7 cells, each 1 mg. wide. This histogram, shown in Figure 2, looks more regular in that it does not show multiple peaks and still shows the bell shape. There is nothing wrong in changing the cell size to bring out the characteristics of the distribution. It would be wasteful to spend time trying

to find reasons for the three peaks in our original histogram when the peaks merely indicate that our sample was too small to fill all the cells evenly. If we make the cells small enough, each unit will fall in a separate cell and we find no bell shape. If we make the cells very wide, all the units fall in the same cell and again we find no bell shape. Decision as to the number of cells to use is a matter for engineering judgment.

If on examining the histogram we decide that the distribution is reasonably normal, we proceed to calculate the mean and the standard deviation. We calculate the mean, $\bar{x}$, as $\frac{1}{N}\sum_{1}^{N} x_i$, where $x_i$ is an individual reading. The mean gain in weight from Table 1 is 379 ÷ 40, or 9.475 mg.

At this point we can reasonably ask whether we can have a great deal of confidence in this mean. If we took another sample of 40 pieces would we get the same answer? We already know that we cannot make two parts exactly alike, and we suspect that the next mean we take may not be exactly the same. To give some insight into this problem, the column means and the row means have been tabulated.

Each column mean is a mean of 10 pieces, each row mean is a mean of 4 pieces, but the variability around this grand mean is much greater for the row means than for the column means. We expect intuitively that the more pieces we average, the closer we will come to the true population mean. It is worth noting, however, how much closer the averages of 10 pieces cluster around the mean than the averages of 4 pieces do. We might expect our averages of 40 pieces to be even more closely bunched around the population mean, and rephrase this to say that we expect that the mean we found from this sample of 40 pieces will not be very far from the true population mean. This population mean is the value which really interests us. The sample mean is taken only to estimate this, and is of no interest in itself. The sample mean is history, the population mean an indication of what will happen in the future.

Having found the mean we are now in a position to calculate the standard deviation, $\sigma$, or rather the square of the standard deviation, which is called the variance. We know if we measure pieces for a given characteristic that the values we find will be scattered about the mean value. It would seem reasonable to calculate the difference of each measured value from the mean $(x_i - \bar{x})$ and then call the average difference from the mean $(x_i - \bar{x})/N$ a measure of the scatter. However, the difference $(x_i - \bar{x})$ is as likely to be positive as negative so the average difference from the mean turns out to be zero. The difficulty obviously springs from the sign of the difference. We get rid of the sign by squaring the value, and calculate:

$$\frac{1}{N}\sum_{1}^{N}(x_i - \bar{x})^2.$$

This expression is called the sample variance, $S^2$, and is an estimate of the population variance, $\sigma^2$.

The variance has been found to be a very useful function. Suppose we combine two or more populations with known variances. The variance of the combination is the sum of the variances of the individual population. For instance we have measured the variances of a set of shafts and of their bearings. The variance of the clearance is equal to the sum of the variances of the shaft and the bearing.

The variance calculations for the plating data are shown in Table 2. This method of computation as shown involves a lot of methodical procedure through a fixed format of calculation, and for this reason other methods have been worked out which give the answer more rapidly. However, it is strongly suggested that anyone starting in the field use the long method until the pattern which the data follow becomes quite familiar.

There are a number of things worth noting in the procedure shown in Table 2. In the first place we rounded our value of $\bar{x}$ from 9.475 to 9.5, because all the x values are given only to one decimal, and presumably the next decimal place is not known. By restricting ourselves to the significant figures, we find only one or two figures in the $(x - \bar{x})$ column, which we can square in our heads and save a lot of work looking up squares. Having calculated the sum of the squares, 61.92, we examine the squares column to see how the values run. We note that the four largest values of $(x - \bar{x})^2$ provide over half the total sum of

**DR. MAURICE PRENDERGAST**
*is Manager of Quality Control Engineering, Semiconductor Division. His background includes four years as a chemistry instructor at the University of Detroit and at Harvard, as well as many years of design and statistical analysis experience for industry. He assumed his present position upon joining Raytheon in 1957. Dr. Prendergast received his A.B., A.M., and Ph.D. degrees in Chemistry from Harvard University in 1930, 1932, and 1937, respectively.*

| | | | | Row Total | Row Mean | Row Range |
|---|---|---|---|---|---|---|
| 9.3 | 10.4 | 8.8 | 9.5 | 38.0 | 9.50 | 1.6 |
| 9.7 | 9.4 | 10.4 | 11.2 | 40.68 | 10.17 | 1.8 |
| 8.2 | 10.6 | 9.4 | 8.5 | 36.72 | 9.18 | 2.4 |
| 10.4 | 9.3 | 8.2 | 5.9 | 33.80 | 8.45 | 4.5 |
| 10.6 | 10.4 | 9.4 | 11.3 | 41.68 | 10.42 | 1.9 |
| 7.4 | 9.3 | 10.2 | 11.3 | 38.20 | 9.55 | 3.9 |
| 10.3 | 6.8 | 9.6 | 8.6 | 35.32 | 8.83 | 3.5 |
| 9.2 | 7.6 | 9.8 | 9.7 | 36.28 | 9.07 | 2.2 |
| 8.8 | 10.7 | 9.1 | 10.5 | 39.12 | 9.78 | 1.9 |
| 9.2 | 8.3 | 12.1 | 9.6 | 39.20 | 9.80 | 3.8 |
| 93.1 Column Total | 92.8 | 97.0 | 96.1 | 379.00 Grand Total | | |
| 9.31 Column Mean | 9.28 | 9.70 | 9.61 | | 9.475 Grand Mean | 2.75 |

Table 1. Gain in Weight on Plating (milligrams)

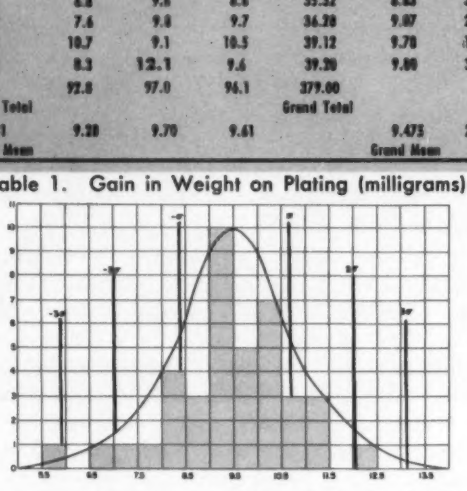

Figure 1. Frequency Histogram of Plating Data with 14 Cells

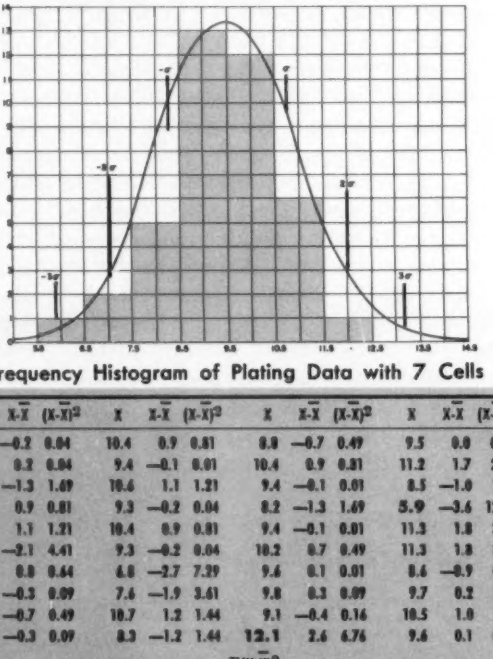

Figure 2. Frequency Histogram of Plating Data with 7 Cells

| X | $X-\bar{X}$ | $(X-\bar{X})^2$ | X | $X-\bar{X}$ | $(X-\bar{X})^2$ | X | $X-\bar{X}$ | $(X-\bar{X})^2$ | X | $X-\bar{X}$ | $(X-\bar{X})^2$ |
|---|---|---|---|---|---|---|---|---|---|---|---|
| 9.3 | −0.2 | 0.04 | 10.4 | 0.9 | 0.81 | 8.8 | −0.7 | 0.49 | 9.5 | 0.0 | 0.00 |
| 9.7 | 0.2 | 0.04 | 9.4 | −0.1 | 0.01 | 10.4 | 0.9 | 0.81 | 11.2 | 1.7 | 2.89 |
| 8.2 | −1.3 | 1.69 | 10.6 | 1.1 | 1.21 | 9.4 | −0.1 | 0.01 | 8.5 | −1.0 | 1.00 |
| 10.4 | 0.9 | 0.81 | 9.3 | −0.2 | 0.04 | 8.2 | −1.3 | 1.69 | 5.9 | −3.6 | 12.96 |
| 10.6 | 1.1 | 1.21 | 10.4 | 0.9 | 0.81 | 9.4 | −0.1 | 0.01 | 11.3 | 1.8 | 3.24 |
| 7.4 | −2.1 | 4.41 | 9.3 | −0.2 | 0.04 | 10.2 | 0.7 | 0.49 | 11.3 | 1.8 | 3.24 |
| 10.3 | 0.8 | 0.64 | 6.8 | −2.7 | 7.29 | 9.6 | 0.1 | 0.01 | 8.6 | −0.9 | 0.81 |
| 9.2 | −0.3 | 0.09 | 7.6 | −1.9 | 3.61 | 9.8 | 0.3 | 0.09 | 9.7 | 0.2 | 0.04 |
| 8.8 | −0.7 | 0.49 | 10.7 | 1.2 | 1.44 | 9.1 | −0.4 | 0.16 | 10.5 | 1.0 | 1.00 |
| 9.2 | −0.3 | 0.09 | 8.3 | −1.2 | 1.44 | 12.1 | 2.6 | 6.76 | 9.6 | 0.1 | 0.01 |

$$\Sigma(X-\bar{X})^2 = 61.92; \quad \frac{\Sigma(X-\bar{X})^2}{N} = 1.548 = s^2$$

$$\sigma^2 = \frac{N}{N-1}\, s^2 = \frac{40}{39}\, s^2 = 1.588 \qquad \sigma = \sqrt{1.588} = 1.26$$

1 $\sigma$ limits: 9.5 ±1.26 or 8.3 to 10.7 — 5 below, 4 above
2 $\sigma$ limits: 9.5 ±2.52 or 7.0 to 12.0 — 2 below, 1 above
3 $\sigma$ limits: 9.5 ±3.78 or 5.7 to 13.3

Table 2. Variance Calculations for Plating Data

the squares. This is typical in data analysis. Most of the variance comes from the relatively few outlying values. Realizing this, we should become very careful in editing data. If we edit out the end values of our distribution we make the data look much better than they really are. We should never discard a measurement unless there are sound statistical reasons for believing that it does not come from the population under study.

Because most of the variance comes from the outlying members of the sample, small samples tend to underestimate the population variance. Since it is unlikely that a small sample will contain a member from the tail of the population, a correction for this is made by multiplying the sample variance by $n/(n-1)$ (where n is the number in the sample) to get an estimate of the population variance. This is Bessel's correction, and should always be used for small samples.

Note also that the sum of the difference columns $(x-\bar{x})$ is $-1.0$. This is to be expected since we used 9.5 for the means instead of 9.475, and so lost 0.025 for each of 40 items. If we had carried three decimal places, the sum of these columns would have been zero.

We now go back to the histogram (Figure 1) and look at the distribution and the sigma limits. From the properties of the normal curve we expect 68 per cent of the distribution to lie between $\bar{x} \pm \sigma$; i.e., between 8.3 and 10.7. On the histogram we find 25 units which lie entirely within these limits and 7 borderline units which we estimate by eye to be 40 per cent within the boundary. This gives a total of 28 units out of 40 or 70 per cent, which is a pretty good check. We expect 95 per cent of our units to lie between $\bar{x} \pm 2\sigma$; i.e., between 7.0 and 12.0. We find 37 out of 40 units, or 92.5 per cent within these limits, which is a fair check. We expect only 3 units in 1000, (i.e., none in 40) to lie beyond the 3-sigma limits, 5.7 to 13.3. Looking at the extreme values in the table we find 5.9 and 12.1, so no units lie beyond the 3-sigma limits. We are now reasonably confident that the sample came from a population having a mean of 9.475 mg. and a standard deviation of 1.26 mg.

Suppose these pieces came from a process specifying plating weight limits of $9 \pm 2$ milligrams. Can parts be made to this tolerance using this process? First we note that 7 mg. corresponds to the $-2$-sigma limit. We know then that 2.5 per cent of the pieces made by the process will be too small to meet the specification. The 11-mg. upper limit lies $1.525 \div 1.26$ sigma above the mean; i.e., at $1.21\sigma$. From a table of areas of the normal curve we find that 11 per cent of the area of the curve lies above $1.21\sigma$. If we use this process and these specifications limits, we find that the process makes 13.5 per cent of the pieces outside the specification limit. What can we do to cut down this loss?

The first step is to center the process. We cut the plating time so the mean weight of plate is 9.0 mg. If this does not change the standard deviation, we now have a process centered at 9.0 mg. with limits at $2.00 \div 1.26$ sigma on each side of the means, or 1.6 $\sigma$. From the table of areas, 5.5 per cent lies outside the 1.6-$\sigma$ limit so we lose 11 per cent. This is not a very great gain in yield, because when we centered we lost nearly as much on the low tail of the distribution as we gained on the high side. The only recourse we have now is to decrease the standard deviation. If we can get sigma down to 1.00 mg. we can get 95 per cent, since our specification limits will then be 2 sigma from the mean. If we get sigma down to 0.67, we should be able to get 99.7 per cent yield providing we keep the process centered. We try better plating bath stirring, rearrange our parts in the bath to improve uniformity of current flow to the parts, and take a distribution after each run to calculate sigma. In this way, we know how the process stands at each step and can stop when it is satisfactory.

Suppose that we have changed the process and now have the correct mean and a satisfactory standard deviation. We cannot then walk away and assume that the process will stay there. On the other hand, we do not want to measure 40 pieces from every batch and go through the calculations each time. How can we keep surveillance over the process without expending a lot of time and effort?

All we really need to be sure of is that the process mean and standard deviation have not changed, and we can do so without taking a sample of 40 pieces. If we take successive samples of $n$ pieces, estimate the mean from each sample, and then make a histogram of these means, we find that the mean of the sample means is the same as the population mean and the sample means are distributed around the population mean with a variance of $\sigma^2/n$, where $\sigma^2$ is the population variance. In other words, the standard deviation of the mean of samples of $n$ pieces from a population is $\sigma/\sqrt{n}$, where $\sigma$ is the population standard deviation. Looking at the row means in the table, each row mean is a mean of 4 pieces, so the standard deviation of these means about the population mean should be $1.26 \div \sqrt{4}$, or 0.63 milligram. From this we conclude that 68 per cent of these row means should lie between the 1-sigma limits of 8.9 to 10.2, 95 per cent between the 2-sigma limits of 8.2 to 10.7, and substantially all between the 3-sigma limits of 7.6 to 11.3. By count, 7 of our pieces lie between 8.9 and 10.2, and all 10 lie between 8.2 and 10.7. We did not have any mean beyond the 2-sigma limits. This is not surprising, since we have only a 5 per cent chance (one in 20) of finding a mean beyond the 2-sigma limit, and we only looked at ten means. If we look at the four column means, our standard deviation for means of 10 pieces is $1.26 \div \sqrt{10}$ or 0.398, and our 1-sigma limits are 9.1 to 9.9, 2-sigma limits 8.7 to 10.3, and 3-sigma limits 8.3 to 10.7. All four averages fall within the 1-sigma limits. We were pretty lucky to have this happen. The probability that any piece would fall within the 1-sigma limits is 0.68, and the probability that 4 out of 4 pieces would fall there is $(0.68)^4$, or about 21 per cent. A statistician would begin to be suspicious if 8 out of 8 pieces fell within these limits, because the probability of this happening is less than 5 per cent.

| Regular Shaft | Hardened Shaft |
|---|---|
| 11 | 7 |
| 8 | 7 |
| 9 | 7 |
| 7 | 10 |
| 7 | 5 |
| 6 | 6 |
| 8 | 6 |
| 6 | 8 |
| 8 | 8 |
| 8 | 7 |

Table 3. Breakaway Torque (gram-cm)

We can display our row averages in the following way. Set up the range covered by the data as the y-axis of a graph and draw horizontal lines at the mean, at the 2-sigma limits of the mean, and at the 3-sigma limits, as shown in Figure 3. For the x-axis we set up the successive readings we have taken, in this case the row numbers, and then plot the value of each mean at its row number. When we do this we see that the points are scattered about the mean in a random fashion. (The lines connecting the points have no meaning, but serve only as guides to the eye in passing from point to point.) This is the way samples should behave. If all the points fell on the mean line, or if they showed any other type of regular behavior, we should become suspicious.

Suppose now we want to control our plating process as it stands with a mean weight of plate per piece of 9.5 mg. and a standard deviation of weight of 1.26 mg. We plate a batch of pieces, take a sample of four pieces at random, determine the gain in weight for each piece, take the mean gain and plot it on our chart. The chart is now called a control chart. We expect to get a pattern similar to that of the row means. In general, we expect the points to lie between the 2-sigma limits, which are now called warning limits. We expect one point in 20 to fall outside these limits, and are not worried when one does. If the next point is also outside the 2-sigma limits, however, we feel that something is wrong with the process; i.e., that either the mean or the standard deviation has changed. The probability of two successive points being outside the warning limits is one in 400 (one

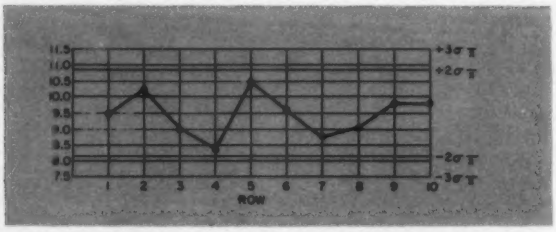


Figure 3. Control Chart for Monitoring Distribution Mean

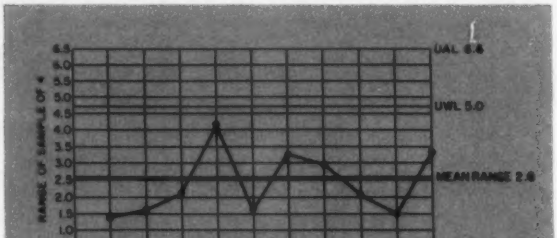


Figure 4. Control Chart for Monitoring Standard Deviation

in 20 squared), and we are unwilling to believe that pure chance gave us the observed result. We will be in error once in 400 batches on the average, and will investigate unnecessarily a process which is operating exactly as it should. Generally, however, we find that when this condition occurs there is something actually wrong in the process, and correcting this brings the chart back between the 2-sigma limits. Similarly we investigate the process if any point goes beyond the 3-sigma limits, now called action limits. The probability that this will happen is less than 1 in 300, and we feel that this is sufficiently unlikely so that we should investigate at once. Again we will be following a false trail once in 300 batches.

The great advantage of the control chart is that it monitors the process continually. As soon as the process begins to change either in mean or standard deviation, the control chart tells us so that we can investigate at once and correct the trouble before it becomes serious.

The chart we have been considering monitors the mean of the distribution. Since a change in the process can occur in mean or in standard deviation, we need another chart to monitor the standard deviation.

One of the obvious things which changes with the standard deviation is the range of the distribution. If we take samples of two pieces from a distribution with a standard deviation of 1.244 mg., we expect the maximum range we would get would be 6 standard deviations. This would occur, however, only if one of the pieces was at the lower 3-sigma limit, which has a probability of 0.001, and the other at the upper 3-sigma limit, which also has a probability of 0.001. The probability of both happening in a sample of two is $(0.001)^2$, so we expect to get a 6-sigma range only one time in a million. There is also a probability that both pieces will have the same measured value, giving us a range of 0. This probability is much harder to calculate because it could occur in many ways. Both pieces could be near the mean or anywhere else in the distribution, and there are different probabilities for each position. Furthermore, we have to consider the accuracy of measurement so we can decide that both pieces have the same measured value. Essentially we divide our distribution into cells whose width is our error of measurement, calculate for each cell the probability that both pieces in the sample would fall in a given cell, and then sum up over all the cells. The same thing can then be done for the probability that the pieces would be one cell apart, two cells, etc.

This is the sort of calculation that the indefatigable statisticians have been making for a long time and tabulating according to their code. We can use their tables to find that for samples of four pieces the mean range equals 2.059 standard deviations. We can set up a control chart for range in which the mean range will be indicated by a line at $2.059 \times 1.26$, or 2.6 mg. From other tables we find the data to set our warning and action limits. For samples of four, the upper action limit is at 2.57 times the mean range, or 6.6 mg., the upper warning limit at 1.93 times the mean range, or 5.0 mg., the lower warning limit at 0.29 times the mean range, or 9.7 mg., and the lower action limit at 0.10 times the mean range, or 0.3 mg. We set up this chart (Figure 4), and plot the range from each row on it to see how it looks. Note that the limits for the range chart are not symmetrical about the mean. This is connected with the fact that the range has a lower limit at zero. We cannot get a sample in which the range is more than 2.6 mg. smaller than the mean range. The probabilities that we will reach an upper or lower warning limit are the same even though the limits are not equidistant from the mean, and the same is true for the action limits. Note also that the distribution of points on the range chart is like that on the mean chart. All the points seem to be in control.

To use this chart for our process we take the range of the sample of four pieces that we take from each batch (i.e., the difference in plate weight between the sample with the greatest amount of plate and that with the least), and plot the range on our chart. As long as the points fall within the warning limits we feel that the range and, therefore, the standard deviation has not changed. If the points go out of control, we look for the cause and correct it.

Control charts of these types have proven very

valuable for many different kinds of processes. They are most useful when kept at the process point where the operator can see them. Operators get considerable satisfaction out of charts that stay in control, and learn to take corrective action early. Some precautions are usually needed to see that the data are not edited so the control chart will look good, this being a common reaction when the charts are first introduced into a process. After the operators see what the charts do for them, however, they become very much concerned that the charts are properly kept.

Control charts are used in situations where we have a process which grinds data out continuously, and it is intuitively reasonable to use statistics under these circumstances. It is much more difficult to convince people that statistical controls should be used for isolated experiments where only a few data are generated. Yet the latter situation needs statistical control much more than the former. Since a process continues to produce data, it will eventually get into trouble unless it is in control and will be corrected as a result of this trouble. An isolated experiment, however, is done only once, and an engineering decision is made on the basis of the results. If the wrong decision is made, there is no mechanism by which the experiment is repeated, so there is no continuing check on the validity of the decision. It is, therefore, doubly important that statistical checks be made on engineering experiments, so the conclusions drawn from them will have determinable confidence limits.

Suppose we are dealing with a servo motor and are interested in reducing the breakaway torque; i.e., the torque required to start the rotor turning from rest. We feel that this depends on starting friction of the bearings, and that we might get better results if we used a hardened shaft, because it would take a better polish and stand up better to wear. We get ten motors with regular shafts and ten with hardened shafts, run them for enough time so that we think that they will be representative of motors in actual service, and then measure the breakaway torque on each motor. We find the measurement for any given motor highly reproducible, and get the values in Table 3.

The order of entry in the table has no meaning, nor is there any significance that a regular shaft reading and a hardened shaft reading lies in the same row. Cursory examination of the table shows that the readings for the regular shaft are generally higher than those for the hardened shaft, which would seem to indicate that the hardened shaft gives a desirable lower breakaway torque. To get some quantitative information we calculate the mean value of each column and find that the mean breakaway torque for the regular shaft is 7.1 gram-cm., while that of the hardened shaft is 7.1 gram-cm. Can we now say that hardening the shaft reduces breakaway torque by about 10 per cent and proceed to make an economic analysis to find out whether this gain justifies the cost of hardening?

Before we take this rash step we ask ourselves what we are really trying to find. We want to know whether the mean of the population of hardened shafts is better than that of the population of regular shafts. From our measurements we have found that the mean of a sample of ten of one kind differed from the mean of a sample of ten of the other kind. How firmly are we convinced that this difference would be maintained if we took another sample from each population? We have done experimental work and are about to draw conclusions from the results. How much confidence can we have in the conclusions? Note that this does not imply that we lack confidence in the data. We assume that all the measurements were made perfectly and can be checked and found absolutely valid. We are concerned now with validity of the conclusions, not of the data.

The first step in analysis would be to make a histogram for each shaft. We may pick up a clue from a sample of only ten pieces. Each histogram shows a central tendency, and we can sketch in bell curves which seem to be reasonable fits. These curves look very much alike, so we sketch in the curve for a combined distribution and conclude that it looks pretty normal. Perhaps the hardening has no effect on the breakaway torque, the difference in the samples being caused by sampling error and not by any real difference in the shafts. By sampling error we mean that the sample mean is not exactly the same as the population mean.

It is extremely common in data analysis, for the purpose of comparing two processes, to assume that the processes make no difference in the variable under study. This is the so called "null hypothesis." The reason for it is that generally it is easier to show that

| | | Variance Ratio 5% Level | | | | | Variance Ratio 20% Level | | | | |
|---|---|---|---|---|---|---|---|---|---|---|---|
| | | Degrees of Freedom in Larger Variance Estimate | | | | | Degrees of Freedom in Larger Variance Estimate | | | | |
| | | 1 | 2 | 6 | 12 | 24 | ∞ | 1 | 2 | 6 | 12 | 24 | ∞ |
| Degrees of Freedom in Smaller Variance Estimate | 1 | | | | | | | | | | | | |
| | 2 | | | | | | | | | | | | |
| | 3 | | | | | | | | | | | | |
| | 6 | | | 3.6 | 3.3 | 3.1 | 2.9 | | | 1.9 | 1.8 | 1.8 | 1.7 |
| | 9 | | | 3.4 | 3.1 | 2.9 | 2.7 | | | 1.8 | 1.8 | 1.8 | 1.7 |
| | 10 | | | 3.3 | 2.9 | 2.7 | 2.5 | | | 1.8 | 1.7 | 1.7 | 1.6 |
| | 40 | | | | | | | | | | | | |
| | 120 | | | | | | | | | | | | |
| | ∞ | | | | | | 1.0 | | | | | | 1.0 |

Table 4. Variance Ratio Table

a hypothesis is false than to prove that it is true. If we can disprove the null hypothesis, we will prove that the processes are different, and can then evaluate the difference. If we cannot disprove the null hypothesis, we need not evaluate the difference because we have no reason to believe that it is meaningful.

Our null hypothesis in this case is that there are no differences in breakaway torque between the population of motors with regular shafts and the population of motors with hardened shafts. How can we disprove it? One approach is to look at the variances of the two populations. We know that if the populations have different variances there is a difference between them. We calculate population variances and find that the regular shafts have a variance of 2.18, while the hardened shafts have a variance of 1.88. Here is a difference, but is it significant? The statisticians have prepared variance ratio tables. We start to look up in the table our ratio of 1.16 (2.18/1.88) and run into a nasty snag. The table is arranged not in terms of number in the sample, but by "degrees of freedom." In the calculation of variances, the degrees of freedom are equal to the number in the sample minus 1. Since our sample size was 10 for each sample, our degrees of freedom are 9.

The variance ratio table has columns headed by the number of degrees of freedom associated with the larger variance and rows headed by the number of degrees of freedom associated with the smaller variance as shown in Table 4. A table is given for each significance level.

We find the column for 9 degrees of freedom is missing, so we take the 12 column because this is the more rigorous test (it shows a smaller variance ratio). At the intersection of row and column we find 3.1 in the table for 5 per cent level of significance. This means that if we took a sample of 10 pieces and estimated the population variance from it, took a sample of 13 pieces from the same population and estimated the population variance from this sample, and we found that the 13-piece sample gave a higher estimate of the variance there would only be a 5 per cent chance that the ratio of the variance estimates would be as great as 3.1. If we found a ratio greater than 3.1 on comparing samples from two sources, we could say that the sources were not from the same population, and 19 times out of 20 we would be correct. But we found a ratio of only 1.6, so we cannot say that the samples are from different populations with 95 per cent confidence. Now you might feel that the statisticians are overly conservative in wanting to be correct 95 per cent of the time, and that you would be willing to make a wrong decision one time out of five. At this point the statistician will remind you that when you get to the 50 per cent level you can be replaced by a coin tosser, and then show you the table at the 20 per cent confidence level. In this table the appropriate value is 1.8, indicating that 20 per cent of the time we would get a variance ratio this great from the specified size samples taken from the same population. Since we did not even get this great a ratio we conclude that there is no significant difference in the variances of the two samples, and that, therefore, they might indeed come from the same population.

Even though the samples cannot be shown to be different from their variances, they might still be from populations with different means. Now we ask, are the differences in sample means significant? Again we frame a null hypothesis, that there is no difference in means. Since we have already found no significant difference in variance, this amounts to saying that the shafts come from populations of identical parameters, which we can think of as one big population with these parameters. We can estimate the mean of this population as the mean of the sample means, which were 7.1 and 7.8 gram-cm.

$$\text{Now:} \quad \bar{x}_1 = \frac{1}{N}\sum_{1}^{N} x_{1i}; \qquad \bar{x}_2 = \frac{1}{N}\sum_{1}^{N} x_{2i};$$

$$\bar{\bar{x}} = \frac{N_1\bar{x}_1 + N_2\bar{x}_2}{N_1 + N_2} = \frac{\Sigma x_{1i} + \Sigma x_{2i}}{N_1 + N_2},$$

where $\bar{x}$ indicates a mean, $\bar{\bar{x}}$ indicates a mean of means or grand average, and the subscripts indicate the sample under consideration.

$$\text{Therefore:} \quad x = \frac{10 \times 7.8 + 10 \times 7.1}{20} = 7\,45 \text{ gram-cm.}$$

We estimate the variance of the population by weighting according to degrees of freedom.

$$\bar{\sigma}^2 = \frac{(N_1 - 1)\,\sigma_1{}^2 + (N_2 - 1)\,\sigma_2{}^2}{(N_1 - 1) + (N_2 - 1)}.$$

$$\text{Since:} \quad \sigma_1{}^2 = \frac{\Sigma\,(x_1 - \bar{x}_1)^2}{N_1 - 1}, \text{ and } \sigma_2{}^2 = \frac{\Sigma\,(x_2 - \bar{x}_2)^2}{N_2 - 1},$$

$$\text{then:} \quad \bar{\sigma}^2 = \frac{\Sigma\,(x_1 - \bar{x}_1)^2 + \Sigma\,(x_2 - \bar{x}_2)^2}{N_1 + N_2 - 2}.$$

Note that we average the variances, not the standard deviations, and that we weight by the degrees of freedom, not by the number in the sample. This is done because it gives results which agree with the facts. Statistics is a highly pragmatic discipline, and tests its methods not by their conformance to some logical structure, but by checking the answers against the facts. This bias toward reality sometimes makes statisticians hard to live with!

From our sample variances we calculate the estimated population variance:

$$\bar{\sigma}^2 = \frac{(N_1 - 1)\,\sigma_1{}^2 + (N_2 - 1)\,\sigma_2{}^2}{N_1 + N_2 - 2},$$

$$= \frac{9 \times 2.18 + 9 \times 1.88}{18} = 2.03.$$

$$\sigma = 1.43 \text{ gram cm.}$$

This is our best estimate of the standard deviation of the population to which we suspect all these shafts belong.

With this value of sigma, we can now calculate the standard deviation of the mean, $\sigma_{\bar{x}}$, of samples of ten. This is $\sigma_{\bar{x}} = \frac{\sigma}{\sqrt{10}}$ or $\frac{1.43}{\sqrt{10}}$, which equals 0.452 gram-cm.

We expect our samples of ten from the population to have means which are normally distributed around the population means with a standard deviation of 0.452 gram-cm. Since our population mean has been estimated at 7.45 gram-cm, we expect that 68 per cent of the samples we take will lie in the range $7.45 \pm 0.452$, 95 per cent in the range $7.45 \pm 0.904$, and substantially all in the range $7.45 \pm 1.356$ gram-cm.

We note that the one $\sigma_{\bar{x}}$ limits are at 7.00 and 7.90, and that both our samples have means within this range. This makes us feel that the difference between the sample means may indeed be sampling error and not reflect a real difference in the two kinds of shafts so far as their breakaway torques is concerned. However, we need some way of stating a confidence limit. Suppose both means had been just beyond the one $\sigma_{\bar{x}}$ limits. There is a 16 per cent chance that a sample mean would lie above the plus one $\sigma_{\bar{x}}$ limit, and an equal chance that the other sample would lie below the minus one $\sigma_{\bar{x}}$ limit. The chance that both would occur simultaneously should be $(0.16)^2$, or 0.0256. We might expect that a difference of two $\sigma_{\bar{x}}$ between the means would occur 2.56 per cent of the time. As a matter of fact, it occurs nearly twice as often. This bothered the statisticians, so the real sampling distribution was determined by Student. To use his tables, first calculate the population standard deviation as above, and then calculate:

$$t = \frac{\bar{x}_1 - \bar{x}_2}{\sigma/N},$$

where $x_1$ and $x_2$ are the sample means, $\sigma$ is the estimated population standard deviation, and N is the number of degrees of freedom used in the estimate of $\sigma$.

In our example: $t = \frac{7.8 - 7.1}{1.43/18} = 2.07.$

We look this value up in a table of $t$ values (Table 5).

We enter the table at the row for 18 degrees of freedom. In any significance column, the value given is the largest value of $t$ you would have the stated probability of getting (because of sampling error) if the two samples came from the same population. For 18 degrees of freedom we would have a 10 per cent chance of getting a $t$ value of 1.73. We had a larger value of $t$, so we can state that the difference in means is significant at the 10 per cent level; i.e., that there was only a 10 per cent chance that we would have seen a value this large if the null hypothesis were true. We might then conclude that the null hypothesis was false and there was a real difference between the regular and hardened shafts. If we said this, we would be right 9 times out of 10. The statistician, who wants to be right 19 times out of 20, would move to the 5 per cent column. Here the required value of $t$ is 2.10, while the value we found is 2.07. The statistician then says that he cannot tell whether there is a difference from the data. In making this statement he is right 19 times out of 20. He will suggest testing more motors and pooling the new information gathered with that already on hand. If as a result of doing this, a $t$ value of 2.11 was found, the statistician would then state that there was a difference and be right 19 times out of 20.

Writing about statistics is like downhill skiing. It is difficult to find a reasonable place to stop. There are so many ways to use the techniques in engineering that pointing them all out would be an endless task. However, the methods discussed — analysis of the normal curve, use of histograms, the variance ratio test, and the $t$-test — are tools so powerful and easy to use that no engineer who employs them will ever make a statement which he cannot defend. An engineering statement, that is.

| Degrees of Freedom | Significance Level | | | | |
|---|---|---|---|---|---|
| | 10% | 5% | 2% | 1% | 0.1% |
| 1 | 6.31 | 12.71 | 31.82 | 63.66 | 636.62 |
| 2 | 2.92 | 4.30 | 6.97 | 9.93 | 31.60 |
| 3 | 2.35 | 3.18 | 4.54 | 5.84 | 12.94 |
| 4 | 2.02 | 2.78 | 3.75 | 4.60 | 6.86 |
| 16 | 1.75 | 2.12 | 2.58 | 2.92 | 4.02 |
| 17 | 1.74 | 2.11 | 2.57 | 2.90 | 3.97 |
| 18 | 1.73 | 2.10 | 2.55 | 2.88 | 3.92 |
| 19 | 1.73 | 2.09 | 2.54 | 2.86 | 3.88 |
| 28 | 1.70 | 2.05 | 2.47 | 2.76 | 3.67 |
| 29 | 1.70 | 2.04 | 2.46 | 2.76 | 3.66 |
| 30 | 1.70 | 2.04 | 2.46 | 2.75 | 3.65 |
| 40 | 1.68 | 2.02 | 2.42 | 2.70 | 3.55 |
| 60 | 1.67 | 2.00 | 2.39 | 2.66 | 3.46 |
| 120 | 1.66 | 1.98 | 2.36 | 2.62 | 3.37 |
| ∞ | 1.65 | 1.96 | 2.33 | 2.58 | 3.29 |

Table 5. Values of t

## Tiny Raytheon "Electronic Package" Will Help Polaris Find Its Target

The most advanced version of the Navy's submarine-launched missile, the deadly Polaris, will locate and destroy its target more than 1200 miles away. Chosen to serve a vital role in the Polaris inertial guidance system were Raytheon Weld-Pak miniature circuit modules. With space at a premium, these lightweight, packaged circuits, based on an M.I.T. Instrumentation Laboratory concept, enable more than 100 components and 300 welds to be packed into each cubic inch. Rugged and ultra-reliable, they are made to endure the shock of launching. Polaris is one of 22 U.S. missiles that rely on Raytheon components and equipment.

Weld-Pak modules, designed and produced by Raytheon, pack more than 100 components and 300 welds into each cubic inch, are exceptionally rugged and reliable.

RAYTHEON

EXCELLENCE IN ELECTRONICS

RAYTHEON COMPANY

WALTHAM, MASSACHUSETTS